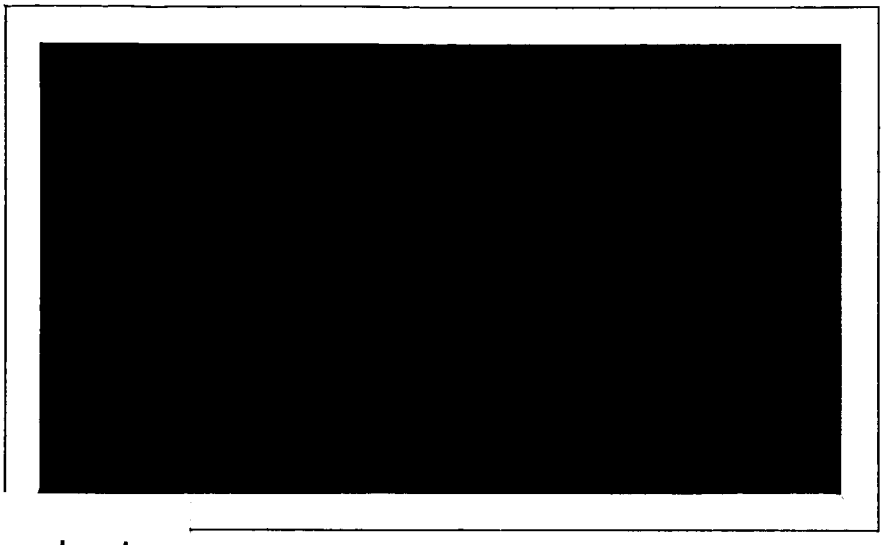

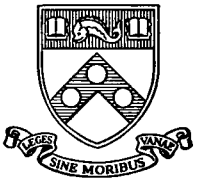

UNIVERSITY OF PENNSYLVANIA

ELECTROCHEMISTRY LABORATORY

PHILADELPHIA, PENNSYLVANIA 19104

SEMI-ANNUAL PROGRESS REPORT

1 MARCH 1964 to 30 SEPTEMBER 1964

STUDIES OF THE FUNDAMENTAL CHEMISTRY, PROPERTIES, AND BEHAVIOR OF FUEL CELLS

NsG-325

Submitted to:

NATIONAL AERONAUTICS AND SPACE ADMINISTRATION

Washington 25, D. C.

Submitted by:

Professor John O'M. Bockris

The Electrochemistry Laboratory

The University of Pennsylvania

Philadelphia, Pa. 19104

TABLE OF CONTENTS

I. DETERMINATION OF POINTS OF ZERO CHARGE

1. Introduction

The radiotracer method for investigation of adsorption was used for the measurement of potentials of zero charge of three more metals, namely, platinum in acid solutions, gold and silver.

2. Experimental and Results

Platinum:

The doubly clad platinum on nickel tape was used. The tape was washed with acetone and was vapor degreased with trichloroethylene. It was further treated with conc. sulphuric acid, washed with water and then threaded through the cell.

The solution in the cleaning compartment of the cell was 0.01 N $HClO_4$ and the adsorption compartment contained 1.8×10^{-5} M naphthalene with appropriate concentration of sodium perchlorate at pH 3. Procedure of anodic and cathodic pulsing followed by a long cathodic pulse was adopted. The tape was washed with deaerated distilled water while transferring it into the adsorption compartment.

The adsorption curves were determined for electrolyte concentrations of 1 N, 0.1 N and 0.01 N sodium perchlorate.

The PZC obtained from intersection of the adsorption vs. potential (N.H.E.) curves for the three coneentrations mentioned is + 470 mv $\pm$ 50 mv (N.H.E.).

Gold

Pure gold tape as obtained from the manufacturer was washed with acetone, vapor degreased with trichloroethylene and further treated with conc. H_2SO_4 for a minute or so. The tape was washed with distilled water and was ready for the experiment.

The solution in the cleaning compartment of the cell was 0.9 N $NaClO_4$ and 0.1 N $HClO_4$ and the naphthalene tracer concentration 1.6×10^{-5} M. A fairly heavy anodic pulse (80 mA/cm^2) for a short time followed by cathodic pulse for a few minutes was found suitable. Again the tape was washed in the middle compartment with deaerated distilled water before it entered into the adsorption compartment.

The adsorption curves were obtained for the electrolyte concentrations of 1 N, 0.1 N and 0.01 N $NaClO_4$.

The PZC obtained from the intersection of the adsorption vs. potential curves is seen to be at 370 mv $\pm$ 50 mv (N.H.E.).

Silver

Pure silver tapes were used. The tape was washed with acetone and vapor degreased with trichloroethylene and without any further treatment it was mounted in the apparatus.

The cleaning solution was 0.8 N $NaClO_4$ + 0.2 N $HClO_4$ and the concentration of C^{14} labeled naphthalene was 1.6×10^{-5} M along with appropriate concentration of sodium perchlorate at pH of 3. As Ag/ClO_4^- system is highly reversible, a small (0.5 mA/cm^2) anodic pulse was passed for a long time. When the tape was about to be drawn out a

cathodic pulse was given. While the tape was moving into the adsorption compartment it was washed with deaerated distilled water.

The adsorption curves have been determined for 1 N and 0.1 N $NaClO_4$ concentrations.

The PZC obtained from the intersections of the adsorption curves is + 70 mv $\pm$ 50 mv (N.H.E.).

The PZC values obtained by this method are in general agreement with the data found in the literature.

Errata

The legends of the figures 1 and 2 of the previous report (1 October 1963 to 31 March 1964) should be as follows:

Figure 1: Dependence on potential of adsorption of naphthalene on nickel (washed with O_2-containing distilled water) in solutions of 0.1 N $NaClO_4$ (0) and 0.01 N $NaClO_4$ (X) at a pH of 13. Concentration of naphthalene 5×10^{-5} M.

Figure 2: Dependence on potential of adsorption of naphthalene on nickel (washed with distilled water free from O_2) in solutions of 0.1 N $NaClO_4$ (X) and 0.01 N $NaClO_4$ (0) at a pH of 13. Coneentration of naphthalene 4×10^{-5} M.

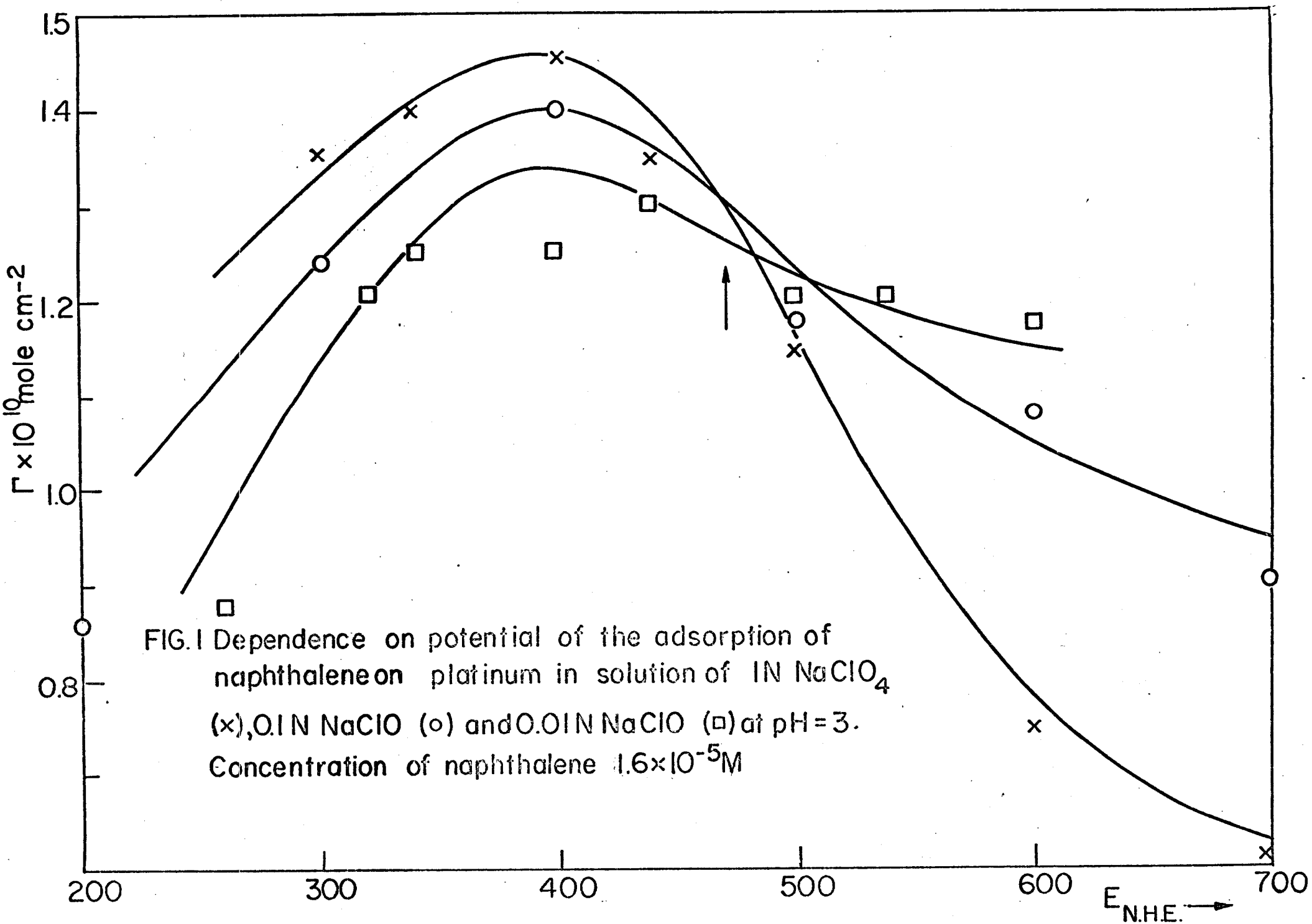

FIG. 1 Dependence on potential of the adsorption of naphthalene on platinum in solution of 1N $NaClO_4$ (x), 0.1 N NaClO (o) and 0.01 N NaClO (□) at pH = 3. Concentration of naphthalene 1.6×10^{-5} M

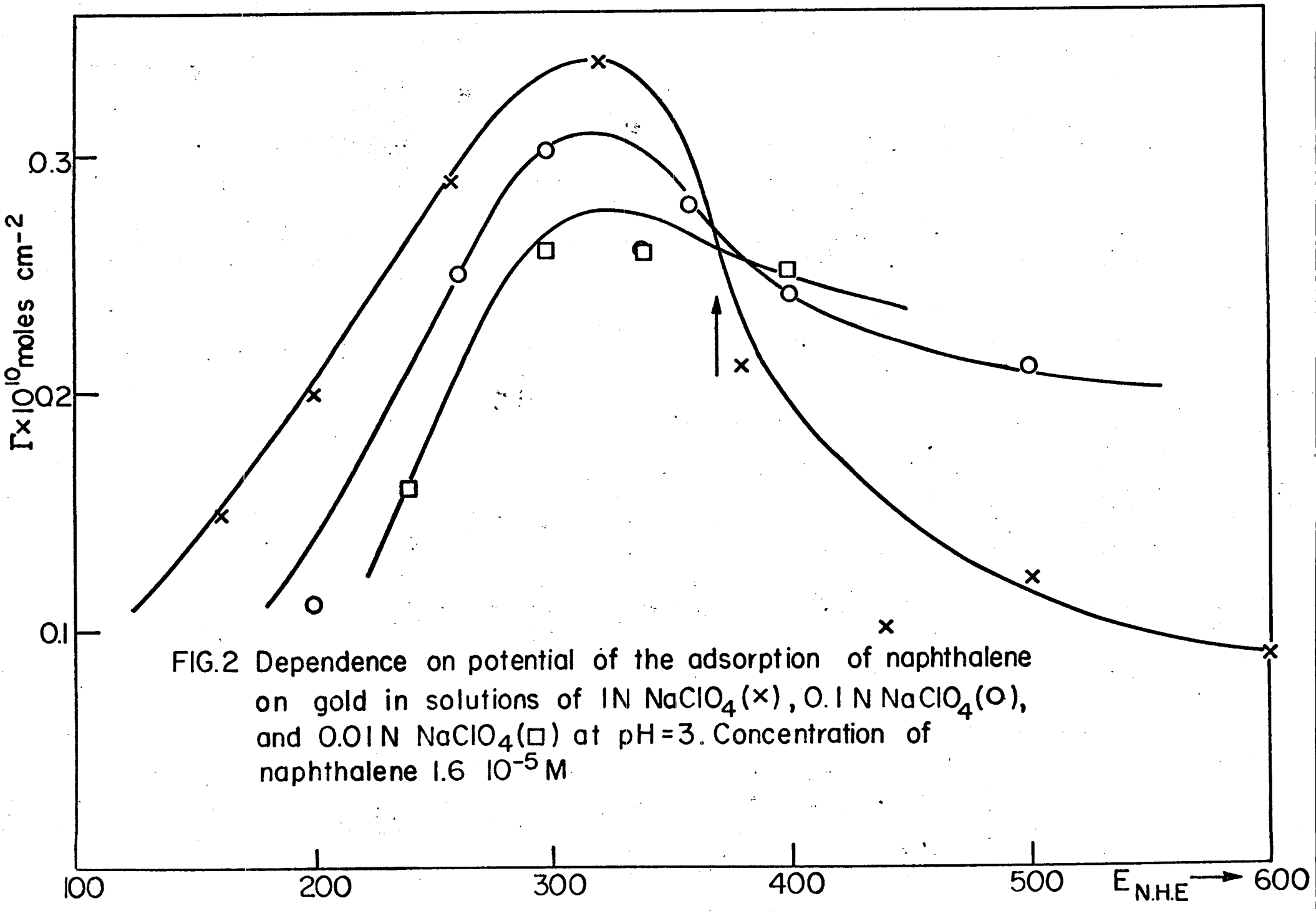

FIG.2 Dependence on potential of the adsorption of naphthalene on gold in solutions of 1N $NaClO_4$ (×), 0.1 N $NaClO_4$ (○), and 0.01 N $NaClO_4$ (□) at pH = 3. Concentration of naphthalene 1.6 10^{-5} M

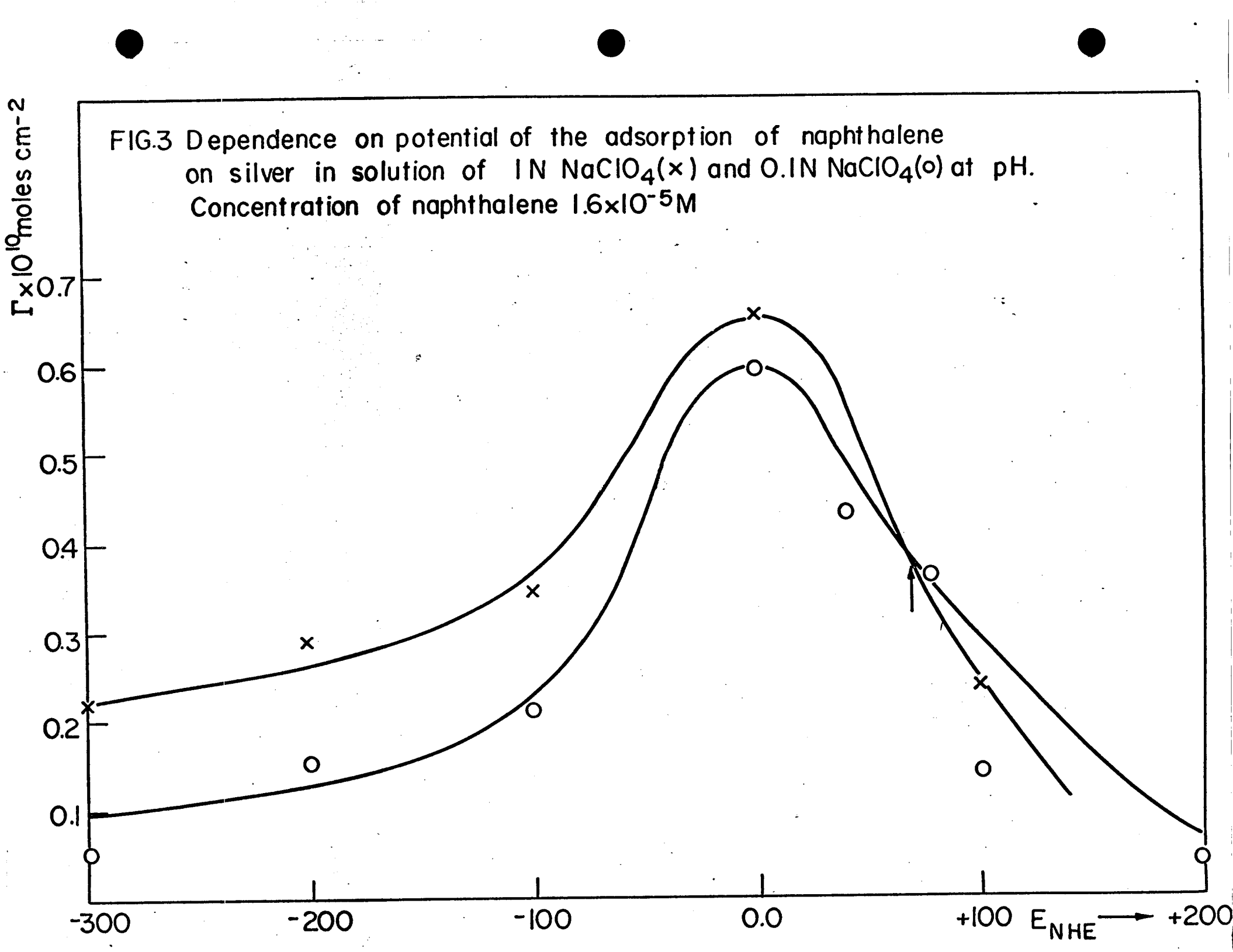
FIG.3 Dependence on potential of the adsorption of naphthalene on silver in solution of 1N $NaClO_4$(×) and 0.1N $NaClO_4$(o) at pH. Concentration of naphthalene 1.6×10^{-5}M
$\Gamma\times10^{10}$moles cm^{-2}
0.7
0.6
0.5
0.4
0.3
0.2
0.1
-300
-200
-100
0.0
+100
E_{NHE} →
+200

II. ELECTROCATALYSIS

A THEORETICAL ANALYSIS OF THE POTENTIAL SWEEP METHOD

1. Introduction

The potential sweep method is essentially an extension of polarographic techniques, in which the potential of a system is controlled externally and is made to vary, usually at a constant rate. It has been applied first as a triangular sweep by Sevcik[1] and the corresponding theory in cases where the reaction is partially or completely controlled by diffusion has been given by Delahay.[2] Application of the method for the study of adsorption of electrochemically active intermediates (i.e. species which can be formed on the surface or removed by steps involving charge transfer) has been made by Will and Knorr[3] who studied the adsorption of hydrogen and oxygen on noble metal electrodes. These authors have derived relationships between the form of the i-V curves observed experimentally and the sweep rate, and interpreted their results qualitatively in terms of the different degrees of irreversibility of the hydrogen and oxygen desorption steps on these metals.

Following the paper of Will and Knorr, the triangular sweep method has been widely used for the study of anodic oxidation reactions relevant to fuel cell technology.[4-12]

The potential sweep method as applied to anodic oxidation of organic fuels, e.g., alcohols,[4-9] organic acids[8,9] and hydrocarbons[11,12] should really be divided into two classes: (1) The slow sweep method with sweep rates in the range of 5 - 50 mV/sec is a quasi-steady state

method where it is hoped (but never proved) that the rate of change of potential with time is slow enough for steady state kinetics to be essentially established, while it is fast enough so that impurities cannot accumulate on the electrode surface and affect the current-potential relationship. (2) The fast sweep method (10^2 - 10^3 V/sec) is a transient method to be compared with galvanostatic transients, intended mainly to measure the concentration of adsorbed species on the surface. The main assumptions made here are that (a) the rate of oxidation is fast compared to the rate of diffusion so that no appreciable readsorption occurs during the transient; (b) the molecules can be removed from the surface only by complete oxidation; (c) the double layer charging current as well as the current used to form an oxide layer on the surface are not affected by the presence of the organic substance in the solution. Of these, only the first assumption can be verified experimentally and the others are unlikely ever to be valid. Moreover, the potential of peak current, often referred to as the "adsorption potential" is an ill-defined quantity which has been shown experimentally[3] and theoretically (see below) to be a function of sweep rate.

The i-V curves obtained by the fast sweep method are equivalent to the differential of the V - t curves obtained galvanostatically. Thus in the range where the Faradaic current is mainly pseudocapacitative (i.e. $i_F = k'd\theta/dt$) we can write $i = CdV/dt$, where C is the sum of the double layer capacity and the adsorption pseudocapacity. With dV/dt - const. the capacity is proportional to the current and the i - t curve observed experimentally is in fact a C - V curve. In comparison the

V- t curve obtained at constant current (galvanostatically) is in fact a V - q plot from which a V - C plot can be obtained, e.g., by electronic differentiation.[13]

In the following sections, expressions are worked out for the current-potential relations wherever possible and so also for the peak potentials and peak currents in the case of some simple anodic and cathodic reactions involving charge transfer. As will be seen below, in the other cases, it is only possible to obtain a numerical solution of the differential equation containing the time (or potential) as an independent variable and the current as the dependent variable. A detailed analysis of the results of the numerical computations now under way will be given in a following report.

2. Theoretical Derivation

A. Anodic Adsorption Reaction

A reaction of the type

$$A^- \longrightarrow A + e_o^- \qquad (1)$$

will be considered. The formation of chemisorbed oxygen from water or the hydroxyl ion is an example of this type.

It is possible to consider several cases for this reaction, depending on whether it is fast or slow and if slow, depending on the regions of potential as well. The observed current-potential relations depend also on the sweep direction (anodic and cathodic). These cases will now be examined.

1. Anodic Sweep

Case (i): Fast reaction (very high exchange current density)

The Faradaic current (i_F) is expressed as

$$i_F = k_1 a_{A^-} (1-\theta) e^{\beta VF/RT} - k_{-1} \theta \, e^{-(1-\beta)VF/RT} \qquad (2)$$

where k_1, k_{-1} are the forward and reverse specific rate constants when metal-solution potential difference V = 0.

θ is the degree of coverage of the electrode with the species A, and a_{A^-} is the activity of the A^- ion at the double layer. Since the reaction is fast,

$$i_F << k_1 a_{A^-} (1-\theta) \, e^{\beta VF/RT} \qquad (3)$$

and also

$$\left| i_F \right| << k_{-1} \theta \, e^{-(1-\beta)VF/RT} \qquad (4)$$

This case is then analogous to that of a charge transfer reaction, considered to be virtually in equilibrium preceding the rate-determining step. The latter has been dealt with by Bockris and Kita[14] and expressions for the pseudo capacity were derived in this work. Under these conditions, equation (2) may be rewritten as

$$0 = k_1 a_{A^-} (1-\theta) \, e^{\beta VF/RT} - k_{-1} \theta \, e^{-(1-\beta)VF/RT} \qquad (5)$$

i.e.

$$\theta/(1-\theta) = K_1 a_{A^-} \, e^{VF/RT} \qquad (6)$$

where

$$K_1 = \frac{k_1}{k_{-1}} \qquad (7)$$

hence

$$\theta = \frac{K_1 a_{A^-} \, e^{VF/RT}}{1 + K_1 a_{A^-} \, e^{VF/RT}} \qquad (8)$$

$$= \frac{K_1 a_{A^-}}{e^{-VF/RT} + K_1 a_{A^-}}$$

The net Faradaic current may also be expressed as

$$i_F = ZF \frac{d\theta}{dt} \tag{9}$$

where Z is the number of equivalents of A per cm^2 of the surface.

From equation (8)

$$\frac{d\theta}{dt} = \frac{K_1 a_{A^-}}{(e^{-VF/RT} + K_1 a_{A^-})^2} \cdot \frac{F}{RT} e^{-VF/RT} \cdot v \tag{10}$$

Since $V = V_o + vt$ where V_o is the initial potential, v the sweep rate and V is the potential at time t. Combining equations (9) and (10)

$$i_F = \frac{zF^2}{RT} \cdot \frac{K_1 a_{A^-} e^{-VF/RT}}{(e^{-VF/RT} + K_1 a_{A^-})^2} \cdot v \tag{11}$$

It may be noted that the expression multiplying v on the right hand side of equation (10) is that for the pseudocapacity, as derived by Bockris and Kita.[14] The total current is given by

$$i = i_F + i_{D,L} \tag{12}$$

In the range of potential where adsorption takes place and θ_{A^-} goes from 0.01 to 0.99 it may be assumed that

$$i_{D,L} << i_F \tag{13}$$

$$i \backsimeq i_F \tag{14}$$

From equation (11) and (14), it follows that at a constant potential,

the current is proportional to the sweep rate. Further, at a constant sweep rate, the current is proportional to the pseudocapacity for this case.

Determination of peak current and potential: Condition for maximum in i - t (or V) curve is

$$\frac{di_F}{dt} = 0 \tag{15}$$

or from (9)

$$\frac{d^2\theta}{dt^2} = 0 \tag{16}$$

$$\frac{d^2\theta}{dt^2} = K_1 a_{A^-} \frac{F^2}{R^2T^2} \frac{e^{-VF/RT}(e^{-VF/RT} + K_1 a_{A^-})^2 - 2e^{-2VF/RT}(e^{-VF/RT} + K_1 a_{A^-})}{(e^{-VF/RT} + K_1 a_{A^-})^4}$$

$$= - K_1 a_{A^-} \frac{F^2 v^2}{R^2T^2} e^{-VF/RT} \left[\frac{e^{-VF/RT} + K_1 a_{A^-} - 2e^{-VF/RT}}{(e^{-VF/RT} + K_1 a_{A^-})^3} \right]$$

$$= - \frac{K_1 a_{A^-} F^2 v^2 e^{-VF/RT}}{R^2T^2} \frac{K_1 a_{A^-} - e^{-VF/RT}}{(e^{-VF/RT} + K_1 a_{A^-})^3} \tag{17}$$

Thus, at maximum

$$e^{-V_M F/RT} = K_1 a_{A^-}$$

$$V_M = - RT/F \ln K_1 a_{A^-} \tag{18}$$

Using equation (18) in (11), the peak current is given by

$$i_{F,M} = (ZF^2/4RT) \cdot v \tag{19}$$

For this case, the peak current is directly proportional to the sweep rate whereas the peak potential is independent of v.

Case (ii): Slow Reactions

(a) General Case

The case considered is the one in which the forward and reverse currents should be taken into account. The current (i_F), as given by equation (2) may be rewritten in the form:

$$i_F = k_1 a_{A^-} e^{\beta VF/RT} - \theta \left(k_1 a_{A^-} e^{\beta VF/RT} + k_{-1} e^{-(1-\beta)VF/RT}\right) \qquad (20)$$

From equation (20)

$$\theta = \frac{k_1 a_{A^-} e^{\beta VF/RT}}{k_1 a_{A^-} e^{\beta VF/RT} + k_{-1} e^{-(1-\beta)VF/RT}} - \frac{i_F}{k_1 a_{A^-} e^{\beta VF/RT} + k_{-1} e^{-(1-\beta)VF/RT}}$$

$$= \frac{k_1 a_{A^-}}{k_1 a_{A^-} + k_{-1} e^{-VF/RT}} - \frac{i_F}{k_1 a_{A^-} e^{\beta VF/RT} + k_{-1} e^{-(1-\beta)VF/RT}} \qquad (21)$$

$$\frac{d\theta}{dt} = \frac{F}{RT} \frac{k_1 a_{A^-} k_{-1} e^{-VF/RT} v}{(k_1 a_{A^-} + k_{-1} e^{-VF/RT})^2} - \frac{\frac{di_F}{dt}}{k_1 a_{A^-} e^{-\beta VF/RT} + k_{-1} e^{-(1-\beta)VF/RT}}$$

$$+ i_F v \frac{k_1 a_{A^-} e^{\beta VF/RT}(\beta F/RT) - k_{-1}(1-\beta)F/RT\, e^{-(1-\beta)VF/RT}}{\left[k_1 a_{A^-} e^{\beta VF/RT} + k_{-1} e^{-(1-\beta)VF/RT}\right]^2} \qquad (22)$$

$$\frac{di_F}{dt} = \frac{F}{RT} \frac{k_1 k_{-1} a_{A^-} v\, e^{-(1-\beta)VF/RT}}{k_1 a_{A^-} + k_{-1} e^{-VF/RT}} + i_F \frac{v\left[k_1 a_{A^-} \beta F/RT - k_{-1}(1-\beta)(F/RT) e^{-VF/RT}\right]}{k_1 a_{A^-} + k_{-1} e^{-VF/RT}}$$

$$- \frac{i_F}{zF} e^{\beta VF/RT} \left(k_1 a_{A^-} + k_{-1} e^{-VF/RT}\right) \qquad (23)$$

The above differential equation (23) cannot be solved analytically.

A numerical solution may, however, be obtained, since it is possible to represent this equation in the form

$$\frac{di_F}{dt} = f(i_F t) \tag{24}$$

It is necessary to have a knowledge of the probable values for the constants in the equation (23) for this purpose.

It is then possible to compare the calculated i - t (or V) curves with the experimental ones and ascertain the correct values of the rate constants and the symmetry factor.

(b) Linear Approximation:

In this case the approximation

$$e^x = 1 + x \tag{25}$$

may be made.

It then follows from equations (2) and (9) that

$$\frac{d\theta}{dt} + \frac{\theta}{ZF}\left[k_1 a_{A^-} + k_{-1} + VF/RT(k_1 a_{A^-} - (1-\beta)k_{-1})\right] = \frac{k_1 a_{A^-}}{ZF}(1 + \beta VF/RT) \tag{26}$$

$$\frac{d\theta}{dt} = \frac{d\theta}{dV} \cdot \frac{dV}{dt}$$

$$= \frac{d\theta}{dV} \cdot v \tag{27}$$

$$\frac{d\theta}{dV} + \frac{\theta}{ZVF}\left[k_1 a_{A^-} + k_{-1} + VF/RT(\beta k_1 a_{A^-} - (1-\beta)k_{-1}\right] = \frac{k_1 a_{A^-}}{ZVF}(1 + \beta VF/RT) \tag{28}$$

Equation (28) cannot be solved analytically. An approximate analytic solution may be obtained using the series method as will be shown below.

Let $$VF/RT = x \tag{29}$$

$$\therefore \qquad F/RT \cdot dV = dx \tag{30}$$

$$dV = RT/F\ dx \tag{31}$$

Using equations (29) to (31) in equation (28)

$$\frac{F}{RT}\frac{d\theta}{dx} + \frac{\theta}{ZvF}\ k_1 a_{A^-} + k_{-1} + x\left(\ k_1 a_{A^-} - (1-\ )k_{-1}\ = \frac{k_1 a_{A^-}}{ZvF}\ (1 +\ x).\right. \tag{32}$$

$$\frac{d\theta}{dx} + \theta\left[A + Bx\right] = C + Dx \tag{33}$$

where

$$A = \frac{RT}{ZvF^2}\ (k_1 a_{A^-} + k_{-1}) \tag{34}$$

$$B = \frac{RT}{ZvF^2}\ \left[\beta k_1 a_{A^-} - (1 - \beta)k_{-1}\right] \tag{35}$$

$$C = \frac{RT}{ZvF^2}\ k_1 a_{A^-} \tag{36}$$

$$D = \frac{RT}{ZvF^2}\ \beta\, k_1 a_{A^-} \tag{37}$$

$$\frac{d\theta}{dx} + \theta(A + Bx) = C + Dx \tag{38}$$

$$\theta = \sum_{n=0}^{\infty} a_n x^n \tag{39}$$

$$\frac{d\theta}{dx} = \sum_{n=1}^{\infty} n a_n x^{n-1} \tag{40}$$

$$\sum_{n=1}^{\infty} n a_n x^{n-1} + A\sum_{n=0}^{\infty} a_n x^n + B\sum_{n=0}^{\infty} a_n x^{n+1} = C+Dx \tag{41}$$

Coefficient of x^o

$$a_1 + Aa_o = C \tag{42}$$

Coefficient of x

$$2a_2 + Aa_1 + Ba_o = D \tag{43}$$

Coefficient of x^2

$$3a_3 + Aa_2 + Ba_1 = o \tag{44}$$

from (42)

$$a_1 = C - Aa_o \tag{45}$$

from (43) and (45)

$$a_2 = \frac{1}{2}\left[(D - Ba_o - Aa_1)\right]$$
$$= \frac{1}{2}\left[D - Ba_o - A(C - Aa_o)\right]$$
$$= \frac{1}{2}\ D - AC + a_o(A^2 - B) \qquad (46)$$

$$a_3 = -\frac{1}{3}(Aa_2 + Ba_1)$$
$$= -\frac{1}{3}\left[\frac{1}{2}\left\{D - AC + a_o(A^2 - B)\right\} + B(C - Aa_o)\right]$$
$$= -\frac{1}{3}\left[\frac{D - AC}{2} + BC + a_o\left(\frac{A^2}{2} - AB = \frac{B_o}{2}\right)\right] \qquad (47)$$

$$\theta = a_o + a_1 x + a_2 x^2 + a_3 x^3 \qquad (48)$$

$$\frac{d\theta}{dx} = a_1 + 2a_2 x + 3a_3 x^2 \qquad (49)$$

$$\frac{d^2\theta}{dx^2} = 2a_2 + 3a_3 x \qquad (50)$$

$$\frac{d\theta}{dt} = \frac{d\theta}{dx} \cdot \frac{dx}{dV} \cdot \frac{dV}{dt}$$
$$= \frac{Fv}{RT} \cdot \frac{d\theta}{dx} \qquad (51)$$

$$\frac{d^2\theta}{dt^2} = \frac{Fv}{RT} \cdot \frac{d}{dt}\left(\frac{d\theta}{dx}\right)$$
$$= \frac{Fv}{RT} \cdot \frac{d}{dx}\left(\frac{d\theta}{dx}\right) \cdot \frac{dx}{dV} \cdot \frac{dV}{dt}$$
$$= \left(\frac{Fv}{RT}\right)^2 \frac{d^2\theta}{dx^2} \qquad (52)$$

Condition for maximum of i vs. t is same as for $d\theta/dt$ vs. t or $d\theta/dx$ vs. x. Thus maximum occurs when

$$x_M = -\frac{2a_2}{3a_3} \qquad (53)$$

Using equations (46) and (47) in (53), the peak potential ($x = VF/RT$) may be found. Using the resulting expression for x_M in (49), the peak current may also be obtained.

(c) Conditions under which reverse current may be neglected

Under these conditions, equation (2) reduces to

$$i_F = k_1 a_{A^-} (1-\theta)\, e^{\beta VF/RT} \tag{54}$$

$$\frac{di_F}{dt} = k_1 a_{A^-} (1-\theta) \frac{\beta vF}{RT} e^{\beta VF/RT} - k_1 a_{A^-} e^{\beta VF/RT} \frac{d\theta}{dt} \tag{55}$$

Condition for maximum is

$$\frac{di_F}{dt} = 0 \tag{56}$$

$$(1 - \theta) \frac{\beta vF}{RT} = \left(\frac{d\theta}{dt}\right)_M$$

$$= i_{F,M}/ZF \tag{57}$$

From equations (54) and (57), it follows that

$$e^{\beta V_M F/RT} = \frac{Z \beta vF^2}{k_1 RT a_{A^-}} \tag{58}$$

$$\therefore \quad V_M = \frac{RT}{\beta F} \cdot \ln \frac{Z \beta F^2}{k_1 RT a_{A^-}} + \frac{RT}{\beta F} \ln v \tag{59}$$

From equation (59), it follows that the peak potential is linearly dependent on the logarithm of the sweep rate. This relation has, indeed, been observed experimentally at higher sweep rates in the case of oxide f mation by Will and Knorr.[3] It is also possible to calculate the chemical rate constant from the intercept of a plot of V_M vs. log v if β is known.

In order to find peak current, equation (54) is made use of. It can be written as

$$ZF \frac{d\theta}{dt} = k_1 a_{A^-} (1 - \theta) e^{\beta VF/RT} \tag{60}$$

$$\frac{d\theta}{1-\theta} = \frac{k_1 a_{A^-}}{ZF} e^{\beta V^{\circ} F/RT} e^{\beta vFt/RT} dt \tag{61}$$

$$\therefore \quad -\ln(1-\theta) = \frac{k_1 a_{A^-}}{ZF} e^{\beta V^{o}F/RT} \frac{RT}{vF} \cdot e^{\beta vFt/RT} + B \qquad (62)$$

where B is a constant.

Let us assume that when $t = 0$, $\theta \longrightarrow 0$

$$0 = A \frac{RT}{\beta vF} + B \qquad (63)$$

where

$$A = \frac{k_1 a_{A^-}}{ZF} e^{\beta V^{o}F/RT} \qquad (64)$$

$$\therefore \quad B = -A \frac{RT}{\beta vF} \qquad (65)$$

$$\therefore \quad -\ln(1-\theta) = \frac{ART}{vF}\left(e^{\beta vFt/RT} - 1\right) \qquad (66)$$

Equation (54) may be written as

$$\ln i_F = \ln k_1 a_{A^-} + \ln(1-\theta) + \beta VF/RT \qquad (67)$$

Using equation (66) and (67)

$$\ln i_F = \ln k_1 a_{A^-} - (ART/vF)\left(e^{\beta vFt/RT} - 1\right) + \beta VF/RT \qquad (68)$$

Equation (68) is of fundamental importance in that it represents the current-potential relation, independent of θ, over the range in which the reverse current may be neglected. Since it is possible to obtain k_1 from a V_M vs. log v plot, knowing β, a theoretical i_F vs. V plot can then be made. Using the equations (58) and (59) which represent V at the peak potential

$$\ln i_F = \ln k_1 - \frac{RT}{\beta vF} \cdot \frac{k_1 a_{A^-}}{ZF}\left(\frac{Z\beta vF^2}{a_{A^-} k_1 RT} - e^{\beta V_o F/RT}\right) + \ln \frac{Z\beta vF^2}{k_1 a_{A^-} RT}$$

$$= \ln \frac{\beta vZF^2}{RT} + \left[\frac{k_1 a_{A^-} RT}{\beta vZF^2} \cdot e^{\beta V_o F/RT} - 1\right] \qquad (69)$$

If in equation (68) the approximation is made that $e^{\beta vFt/RT} >> 1$, and the expression for the peak potential then introduced, it follows that the peak current is given by

$$\ln i_{F,M} = \left(\ln \frac{\beta v Z F^2}{RT} - 1\right) \tag{70}$$

i.e.
$$i_{F,M} = (ZF)\left(\frac{\beta F}{RT}\right) \cdot \frac{v}{e} \tag{71}$$

Under these conditions, too, the maximum peak current is proportional to the sweep rate.

The analytic solution (equation (68)) may be used as a check of the numerical solutions obtained as a computer under the conditions in which the reverse current may be neglected in comparison to the forward current.

2. Cathodic Sweep

When the sweep direction is reversed starting at the highest anodic potential, a similar analysis as in the preceding section (1.1) may be carried out. Only in the case of the highly reversible reaction and in the case of the irreversible reaction in which the anodic current may be neglected is an analytic solution possible. It is worthwhile examining the latter case which is dealt with below.

Expression for current-potential behavior, peak current and peak potential - Region in which anodic current can be neglected

For this case, the Faradaic current is given by

$$i_F = - k_{-1} \theta e^{-(1-\beta)VF/RT} \tag{72}$$

from equation (2). Differentiating equation (72) with respect to time

$$\frac{di_F}{dt} = k_{-1} \theta(1-\beta)\frac{vF}{RT} e^{-(1-\beta)VF/RT} - k_{-1} e^{-(1-\beta)VF/RT} \frac{d\theta}{dt} \tag{73}$$

Condition for maximum is

$$\frac{di_F}{dt} = 0 \qquad (74)$$

i.e. $$\theta (1 - \beta)vF = d\theta/dt$$

$$= \frac{i_{F,M}}{ZF} \qquad (75)$$

since equation (72) holds at the maximum,

$$e^{-(1-\beta)V_M F/RT} = - \frac{Z(1 - \beta)vF^2}{k_{-1} RT} \qquad (76)$$

i.e. $$V_M = - \frac{RT}{(1-\beta)F} \ln \frac{ZF^2(1-\beta)}{k_{-1} RT} - \frac{RT}{(1-\beta)F} \ln (-v) \qquad (77)$$

It must be noted that v is negative during the cathodic sweep and the negative sign within parentheses in the second term on the right hand side is as expected.

Equation (77) is also similar in form to equation (59) but with signs reversed and k_{-1} replacing $k_1 a_{A^-}$. Further, the peak potential becomes more cathodic with increase in sweep rate, as is observed, for example, in the case of oxide reduction on platinum.

It is necessary to know the current-potential relation, independent of θ, in order that the expression for the peak current may be obtained. The method used is similar to that in 1(ii) (c), and is given below.

Rewriting equation (72) using equation (9)

$$\frac{d\theta}{\theta} = - \frac{k_{-1}}{ZF} e^{-(1-\beta)VF/RT} dt \qquad (78)$$

$$V = V_{o,2} + vt \qquad (79)$$

where $v < 0$

$$\frac{d\theta}{\theta} = - \frac{k_{-1}}{ZF} e^{-(1 - \beta)V_{0,2}F/RT} e^{(1 - \beta)vFt/RT} dt \qquad (80)$$

$$\ln \theta = \frac{k_{-1}}{Z\mathcal{F}} e^{-(1-\beta)V_{0,2}\mathcal{F}/RT} \quad \frac{RT}{(1-\beta)v\mathcal{F}} e^{(1-\beta)v\mathcal{F}t/RT} + \text{const.} \tag{81}$$

Assume that at $t = 0$, $\theta \longrightarrow 1$. Thus,

$$\text{const} = - \frac{k_{-1} RT}{(1-\beta)Zv\mathcal{F}^2} e^{-(1-\beta)V_{0,2}\mathcal{F}/RT} \tag{82}$$

$$\therefore \quad \ln \theta = - \frac{k_{-1} RT}{(1-\beta)Zv\mathcal{F}^2} \left[e^{-(1-\beta)V\mathcal{F}/RT} - e^{-(1-\beta)V_{0,2}\mathcal{F}/RT} \right] \tag{83}$$

$$\begin{aligned} \ln i_F &= \ln k_{-1} + \ln \theta - (1 - \beta)V\mathcal{F}/RT \\ &= \ln k_{-1} + \frac{k_{-1} RT}{(1-\beta)Zv\mathcal{F}^2} \left[(e^{-(1-\beta)V\mathcal{F}/RT} - e^{-(1-\beta)V_{0,2}\mathcal{F}/RT} \right] \\ &\quad - (1 - \beta)V\mathcal{F}/RT. \end{aligned} \tag{84}$$

Equation (84) represents the current-potential relation during a cathodic sweep for the case in which the anodic current may be neglected. This equation is similar in form to equation (68) which is that for the corresponding case in the anodic sweep.

Using equation (77) in (84), the peak current is given by

$$\begin{aligned} \ln \left| i_{F,M} \right| &= \ln k_{-1} + \frac{k_{-1} RT}{(1-\beta)Zv\mathcal{F}^2} \left[- \frac{Z(1-\beta)v\mathcal{F}^2}{k_{-1} RT} - e^{-(1-\beta)V_{0,2}\mathcal{F}/RT} \right] \\ &\quad + \ln \frac{Z\mathcal{F}^2(1-\beta)}{k_{-1} RT} + \ln(-v) \\ &= \ln \left[\frac{Z\mathcal{F}^2(1-\beta)(-v)}{RT} \right] - \left[\frac{k_{-1} RT\, e^{-(1-\beta)V_{0,2}\mathcal{F}/RT}}{(1-\beta)Zv\mathcal{F}^2} + 1 \right] \end{aligned} \tag{85}$$

If the approximation is made that the first term within the second square brackets is small compared to unity ($V_{0,2}$ is large and positive), then

$$\ln \left| i_{F,M} \right| = \ln \frac{Z\mathcal{F}^2(1-\beta)(-v)}{RT} - 1 \tag{86}$$

$$i_{F,M} = e^{-1} \frac{Z\mathcal{F}^2(1-\beta)(-v)}{RT} \tag{87}$$

i.e. $$i_{F,M} \propto (-v). \qquad (88)$$

Equation (88) is identical with (71) except that $(1-\beta)$ replaces β and $(-v)$ replaces $(+v)$.

3. Conclusions

An analytic solution of the differential equation

$$\frac{di_F}{dt} = f(i_F, t)$$

is possible only in the case of very fast reactions or where the cathodic current can be neglected in the anodic sweep and the anodic current in the cathodic sweep.

In the former case, the peak potential is independent of the sweep rate but the peak current varies linearly with the sweep rate. In the latter case, the peak potential varies with the logarithm of the sweep rate and the peak current varies linearly with the sweep rate. These semi-logarithmic relationships between V_M and log v have been observed experimentally by Will and Knorr[3] in the case of the oxide formation and reduction reactions. In these cases, it is possible to obtain values of the rate constants if β is known.

(ii) In regions where both forward and reverse current have to be taken into account, it is necessary to carry out a numerical analysis independent of whether the exponential terms involving the potentials can be linearized or not. In the case where the exponential terms can be linearized, it is possible to obtain a series solution. In the case of a numerical analysis it is necessary to use various values of k_1, k_{-1}, β and obtain a plot of i_F vs. V(or t) as a function

of sweep rate and compare with the corresponding experimental i - V (or t) curves. Alternatively values of k_1, k_{-1} obtained in the regions where the reverse currents may be neglected may be used for the numerical analysis and then a comparison made with the experimental values.

4. Future work

(i) The differential equations in i and t for the case in which both the forward and reverse currents have to be taken into account will be solved numerically on a computer for the oxide formation and reduction reactions. The theoretical results will then be compared with the data of Will and Knorr.

(ii) A theoretical analysis for a cathodic adsorption reaction will be made on the same lines as for the anodic adsorption reaction. In this case, a reaction of the type

$$C^+ + e_o^- \longrightarrow C$$

$$2C \longrightarrow C_2$$

will also be examined (e.g., the hydrogen evolution reaction).

(iii) The experimental results for more complex reactions, e.g., methanol or formic acid oxidation will then be examined theoretically.

References

1. Sevcik, A., Colln. Czech Chem. Comm., 13, 349 (1948).

2. Delahay, P., "New Instrumental Methods in Electrochemistry, Chapter 6), Interscience Publishers, Inc., N. Y. (1954).

3. Will, F. G., and Knorr, C. A., Z. Elektrochem., 64, 258 (1960).

4. Buck, R. P., and Griffith, L. R., J. Electrochem. Soc., 109, 1005 (1962).

5. Vielstich, W., Z. Instrumenten. 71, 29 (1963), Chem. Ing. Tech., 35, 362 (1963).

6. Gilman, S., and Breiter, M. W., J. Electrochem. Soc., 109, 1099 (1962).

7. Breiter, M. W., Electrochim. Acta, 8, 973 (1963).

8. Giner, J., Electrochim. Acta, 9, 63 (1964).

9. Bagotskii, V. S., Vasilyev, Yu. B., Electrochim. Acta, 9, 869 (1964).

10. Gilman, S., J. Phys. Chem., 68, 70 (1964).

11. Savitz, M. L., and Frysinger, G. R., Electrochem. Soc., Extended Abstracts of Battery Division 9, 24 (1964).

12. Rhodes, D. R., Ibid, 9, 36 (1964).

13. Conway, B. E., and Angerstein-Kozlowska, H., J. Electroanal. Chem. (1964)

14. Bockris, J. O'M., and Kita, H., J. Electrochem. Soc., 108, 676 (1961).

III. CATALYTIC ACTIVITY FOR SIMPLE ELECTRODE REACTION

Nature of the Catalyst Surface

I. Introduction

The effect of grain size of an inert metal electrode on the rate of simple electrochemical reactions has been studied and preliminary results in the study are given in the last Report. As an inert electrode, platinum was chosen and simple reactions, such as Fe^{2+}/Fe^{3+} and hydrogen reaction, were chosen. No effect of grain size in either case has been observed.

This work has been extended to include three crystallographic planes of platinum single crystals. Only hydrogen evolution reaction has been studied. In the second part of this Report continued work on the catalytic activity on various substrates is described. It includes activities for hydrogen reaction on metals in alkaline solutions.

2. Experimental

Three single crystals in the form of cylinders with the basal planes corresponding to (100), (110) and (111) planes, were fitted into hollow cylindrical Teflon holders and suspended into the solution by Pt wires.

The single crystals were mechanically hand polished by α - polishing alumina (0.3 μ). Polishing was done for about 1/2 hour when the surface of the crystal looked bright. Thereafter crystals were electro-etched to reveal undamaged crystal planes. The electro-etching was done by alternating current in a solution of 20% HCl saturated with

NaCl. The time of etching was approximately 30 minutes. Pt wire was used as a counter electrode. Solution was magnetically stirred. After etching, crystal was thoroughly washed by flowing conductivity water.

Solution preparation was done in the same way as described in the previous Report. During the pre-electrolysis, crystals were kept above the solution in hydrogen atmosphere. After pre-electrolysis, the electrode was dipped into the solution and the cathodic Tafel lines were determined. Bubbling of H_2 gas in the test electrode compartment tended to block the single crystal surface and increase resistance to current flow. To avoid this, measurements were carried out under unstirred conditions. The data are given in Table 1. It can be seen from the table that the rates were essentially the same at all three crystals.

These results, combined with the previous results on electrodes with various grain sizes, can be taken to indicate that grain size and orientation of grains do not affect the rate of simple reactions considered.

TABLE 1

TAFEL PARAMETERS ON VARIOUS PLANES OF PLATINUM

Crystal	b(mV)	i_o(A/cm^2)
(111)	60 - 75	1.4×10^{-3}
(110)	55	9×10^{-4}
(100)	55	9×10^{-4}

3. Catalytic activity of various metals in alkaline solutions

Catalytic activity for hydrogen reaction has been determined on a number of metal electrodes in alkaline solution. Extreme precautions have been taken in preparation and purification of solution. Concentrated Baker analytical grade NaOH solution was recrystallized three times in H_2 atmosphere. The solution was cooled in methanol mixed with dry ice. Excess of the solution in crystallization was discarded by sucking out. The crystals were allowed to melt and then they were again recrystallized. Finally the pure conc. NaOH solution was withdrawn in a calibrated tube fitted with ball joints. The solution was standardized by taking an aliquot portion and titrating with HCl solution. Then the proper amount was directly transferred to the cell and a 0.1 N solution was made. This work is under way and as of yet no conclusions have been drawn from the results in alkaline solution.

IV. DEACTIVATION OF ELECTRODES

In the last Report, preliminary results are given for the galvanostatic polarization studies of deactivation of platinum electrodes during electro-reduction of dissolved oxygen in 1 N sulfuric acid solution. Assuming a pseudo steady state at any given instant, and making use of the nature of polarization curves obtained at different current densities and time intervals, the change of apparent exchange current density of the reaction with time has been obtained. It was found that the exchange current density decreases by nearly one power of ten in the course of about 50 hours. These results indicated that "impurity effect," or "poisoning" of the electrode, is the cause of deactivation. Further study was, however, necessary to evaluate the exact causes of deactivation in the system under investigation.

In the first part of this Report, studies were described of the deactivation of platinum electrodes in oxygen dissolution and, in the second, for ethylene oxidation reactions.

1. Deactivation in oxygen reduction

1.1 General

If impurities from the solution are the cause of deactivation of the electrode, there are, presumably, two modes in which this can happen.

(a) Impurities generated during the electrode reaction, or impurities spuriously added to the system primarily through the saturating gas, may directly participate in electrochemical redox reactions at the metal solution interface. This will result in the change of

mechanism from 'one electrode reaction controlling the potential' to 'two or more reactions controlling the potential'. Thus, the net effect depends on the redox state of impurity, its concentration in solution, and also on the extent of adsorption depending upon the electrode potential.

(b) Alternatively, impurities may poison the electrode by masking the electrode area with a non-conducting film. In this case, the effective area of the electrode is reduced and thus the observed overpotential for the same current increases.

In either mode of deactivation the extent of adsorption (θ), depends on the electrode potential. If one starts with a fresh surface during galvanostatic polarization experiments, one observes a change in potential. The change in potential in turn causes a shift in adsorption characteristics of impurities. From this point of view, it is difficult to evaluate the true extent of 'poisoning'. Under such circumstances, it is desirable to study deactivation under constant potential conditions.

1.2 Experimental

An experiment on deactivation may last for one to two weeks. In order that sufficient data are collected in reasonable time, it was decided to run a larger number of experiments ($\sim 4 - 6$) simultaneously. For this purpose, two procedures for potentiostating have been used. In the first, a relatively low impedance potentiometer is used as a voltage source between the working electrode and counter electrode.

For this, a non-polarizable counter electrode is used. Currents of the order of 10^{-3} to 10^{-4} amps are possible, if hydrogen electrode

is used as the counter electrode. The requirement is, however, low resistance between the counter and the test electrode. In Figure 1 a cell developed for this purpose is shown. It consists of two compartments, (A) and (B). The latter compartment is placed inside the (A) compartment. Solutions in both compartments are separated by a coarse frit (to minimize resistance). The working electrode compartment A has provisions for oxygen bubbling and mounting of the test electrode. Compartment (B) contains counter electrode, which serves also as a reference electrode. This electrode is a palladium U-tube through which hydrogen is flowing. Nitrogen was bubbled in compartment (B) to sweep away oxygen that might be diffusing from the test electrode compartment (A) towards the reference electrode.

The system seemed to work well, but the following difficulty developed. Nitrogen bubbled in the reference electrode compartment was not fully efficient in removing the oxygen diffusing to reference electrode. Reduction of oxygen at the palladium reference electrode resulted in the production of H_2O_2. As experimentally found, H_2O_2 formed in the reference electrode compartment (A), diffused back into the working cell (B). Since the spurious addition of H_2O_2 to the system is not desirable, particularly for the long time study of the deactivation, this set-up had to be discarded. Other reference electrodes, like $Hg/HgSO_4$, Ag/AgCl, etc., were found unsuitable, mostly due to their solubility and contamination of test solution.

In the second series of experiments Philbrick operational amplifiers (35A) were used to build potentiostats (four). The potentiostat consists of a high gain, d.c. differential operational amplifier

connected with negative feedback. Any departure of the reference electrode potential from the preset potential (i.e. standard e.m.f.) is amplified and applied (sign inverted) to the auxiliary electrode, thus correcting the initial departure. The block diagram of the potentiostat working with a single Philbrick power supply is given in Figure 2.

In order to maintain high purity conditions throughout the course of experiments over two weeks, and to distinguish between 'recrystallization' and 'poisoning' theories of deactivation, it is necessary to subject the test solution to continuous pre-electrolysis. Continuous change of solution would involve elaborate arrangements and was discarded as a method. Cells previously used for galvanostatic polarization have been modified to allow for continuous pre-electrolysis.

The main feature of the new cell arrangement (Fig. 3) is that solution from test electrode compartment flows along all glass closed system into the pre-electrolysis compartment. Between the test electrode and the pre-electrolysis compartments, an all glass centrifugal pump with magnetic stirrer is situated. A constant level head is provided in the pre-electrolysis cell, so that the same volume of the solution leaves the pre-electrolysis compartment as enters it. This arrangement maintained a constant solution level in the test-electrode compartment. The solution overflowing through the constant level in the pre-electrolysis cell flows back into the test cell. The rate of circulation could be controlled by changing the speed of rotation of the magnet. Other features of the cell, not shown in the diagram, consisted of gas inlets and outlets, water sealed stopcocks, counter and reference electrode compartments.

The present stage of the work along these lines stands at a point where arrangements have been made for actual measurements. Experiments have been designed to carry out deactivation studies on well annealed and strained electrodes in presence and absence of impurities in order to evaluate factors causing deactivation of electrodes.

2. Deactivation of electrodes by capacitance measurement

2.1 Introduction

It is known experimentally that the activity of platinized Pt electrode decreases with time, causing a decrease in current density at a constant potential during anodic oxidation of organic compounds. It was observed independently in this laboratory that the ionic double layer capacity decreases also with time in a manner which can be qualitatively related to the decrease in current. The manner in which the capacity changes with time has been examined under various conditions and the results are given below.

2.2 Experimental

Experiments were carried out at 25°C when capacity was measured in the presence of N_2, and at 80°C when both current and capacitance were measured in the presence of ethylene. An usual 3-compartment pyrex cell was used with stopcocks separating the working electrode compartment from the counter and reference electrode compartments. A mercury-mercurous sulfate reference electrode was used, and platinized Pt electrodes served as working and counter electrodes. The working

electrode was activated by anodic and cathodic pulsing externally or in the cell. In the latter case care was taken to avoid extensive gas evolution. Activation outside the cell was terminated by prolonged cathodic polarization.

Capacitance measurements were made by applying a large galvanostatic pulse to the electrode which was originally held at + 0.50 V N.H.E. The block diagram of the circuit is shown in Fig. 4. Initially, the potentiostat and galvanostat were connected in the circuit with the former taking up all the current produced by the latter. Galvanostatic control is attained by opening a single switch which disconnects the potentiostat from the circuit.

For high purity runs, triple distilled water was re-distilled into the cell under nitrogen atmosphere through an all glass system. Transistor grade sulfuric acid was used to make 1 N solution. Cathodic pre-electrolysis was carried out at 0.1 Amp. for 20 hours, followed by anodic polarization at 0.5 volt for 10 hours. By the end of this treatment the anodic current density was no more than 0.2 μ Amp..

2.3 Results

Fig. 5 shows the change of capacity and of current at constant potential (0.62 V N.H.E.) as a function of time in the ethylene saturated solution. Both quantities are seen to decrease with time (though not at the same rate) for about 5 days. The same results are plotted again in Fig. 6 as C/i versus time. The ratio remains essentially constant over the first ten hours and then increases with time.

Plots of the variation of capacitance with time in solutions

through which only nitrogen was bubbled are given in Fig. 7. A comparison between regular and highly purified solution is shown. The effect of addition of $(C_3H_7)_3N$ into the highly purified solution is also shown. A better comparison is obtained in Fig. 8 where the relative values of the capacitance (in this case C/C_{1000} where C_{1000} is the value obtained after 1000 min. under any one set of conditions) are plotted. While two linear sections appear to exist on the C - log t plot, a single straight line is obtained when C is plotted vs. $t^{-1/2}$, as shown in Fig. 9a, b and c. This result does not seem to depend on the presence of impurities, as seen by comparison of Fig. 9b and 9c.

2.4 Discussion

The decrease in ionic double layer capacity is associated with a decrease in real surface area (or roughness factor) probably due to surface rearrangement. Support for this view is obtained from the fact that the phenomenon is independent of solution purification. The effect cannot be due to hydrogen absorbed in the metal since the pseudocapacity arising from this is proportional to the hydrogen ionization current at a constant potential. The latter cannot exceed the observed residual current which is less than 1% of the applied galvanostatic pulse.

A slow rearrangement of the platinum surface following activation by anodic and cathodic pulsing is to be expected. Thus a phase oxide is undoubtedly formed during anodic polarization at high potentials (> 1.8 V) and when it is reduced rapidly during the cathodic cycle, a long time may lapse before the equilibrium configuration of the Pt atoms is regained. The constancy of the C/i ratio shows in Fig.6 over

a period of time is an indication that the decrease in current is due here to a decrease in available surface area, with no change in current density. The subsequent rise of C/i does, however, indicate that other factors play a role in decreasing the current density at constant potential.

We note that the time effects do not depend on solution purification. Addition of an impurity into the solution decreases the absolute value of the capacity substantially (Fig. 4) as expected, but when the curves are normalized (Fig. 5) to have the same value at 1000 min., the effect of impurity is rather small.

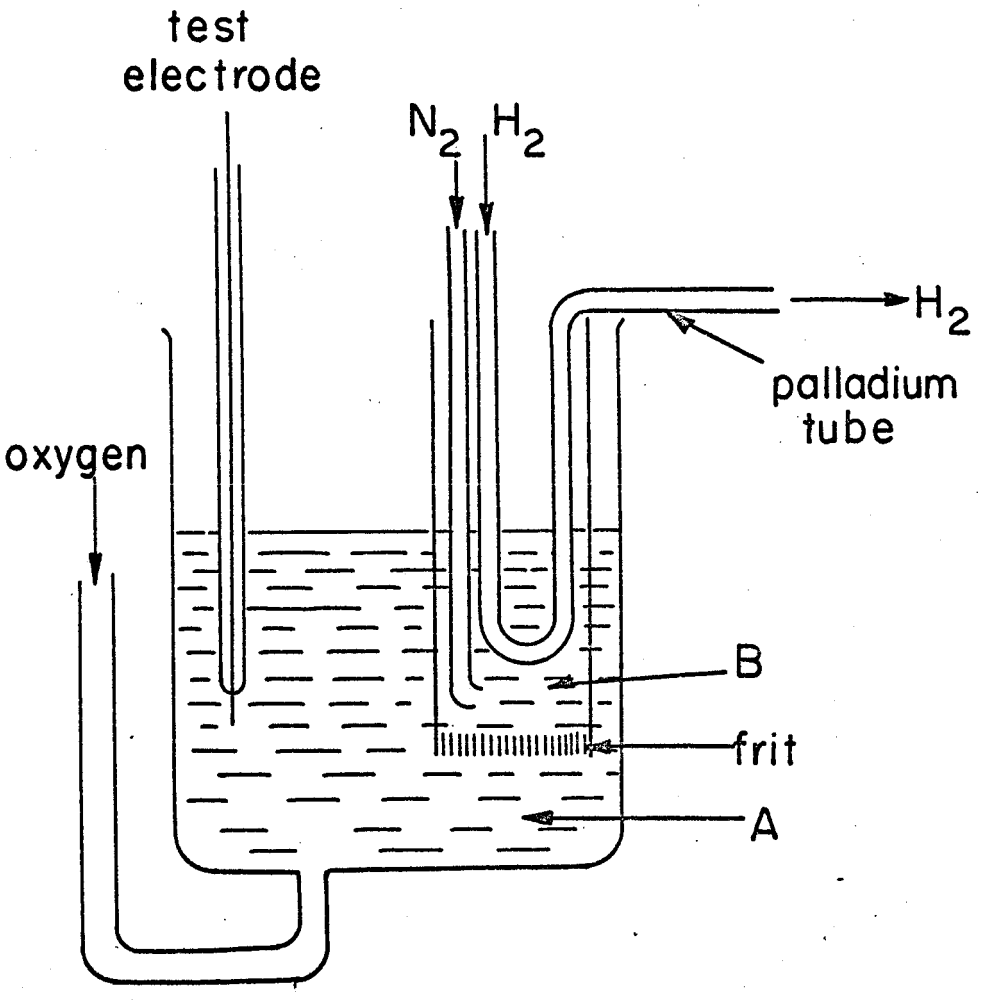

FIG. 1

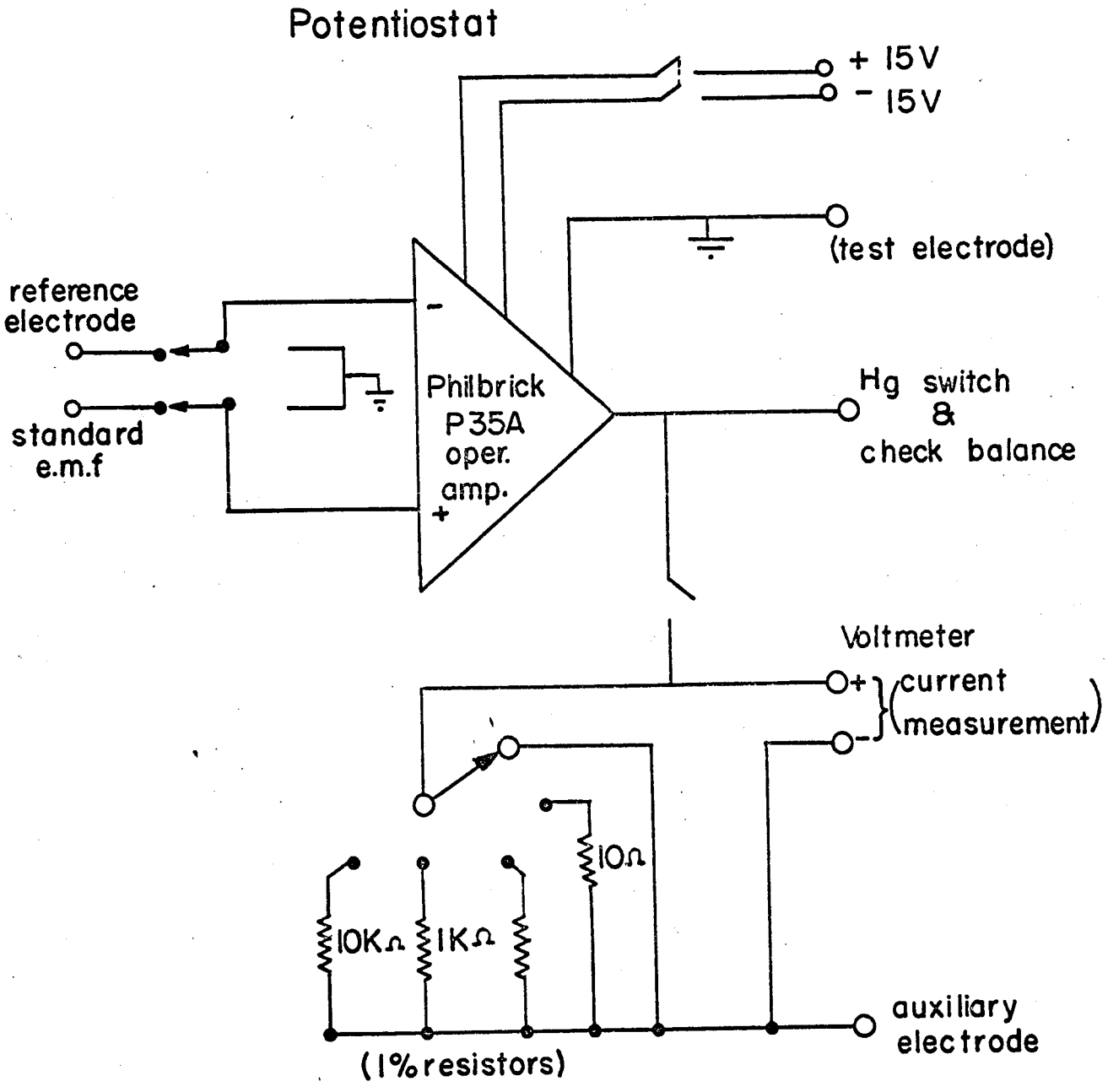
Potentiostat
+ 15V
- 15V
(test electrode)
reference electrode
standard e.m.f
Philbrick P35A oper. amp.
Hg switch & check balance
Voltmeter
current measurement
10Ω
10KΩ
1KΩ
auxiliary electrode
(1% resistors)

FIG.2

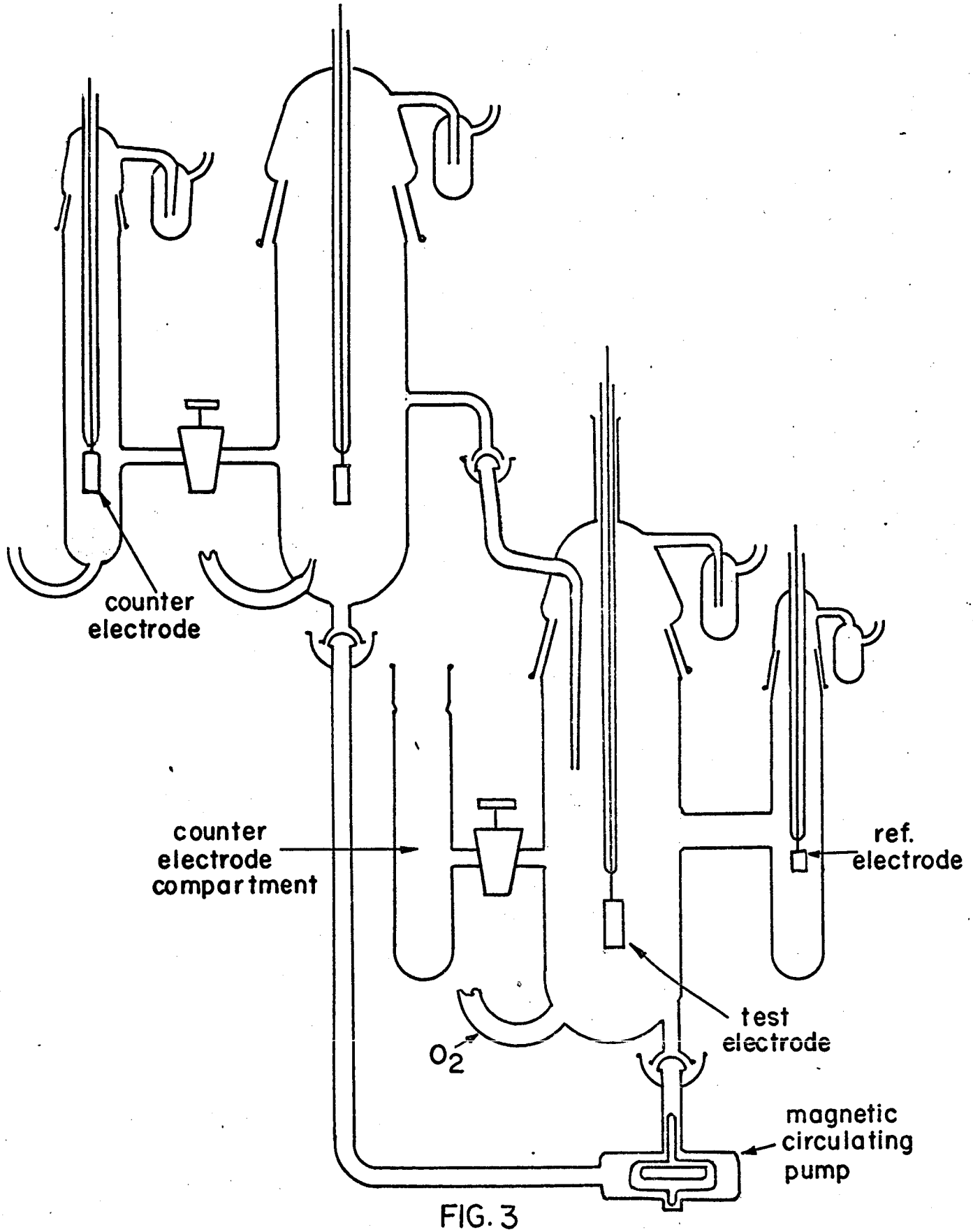
counter electrode
counter electrode compartment
ref. electrode
test electrode
O_2
magnetic circulating pump

FIG. 3

FIG.4 Circuit for capacitance measurements

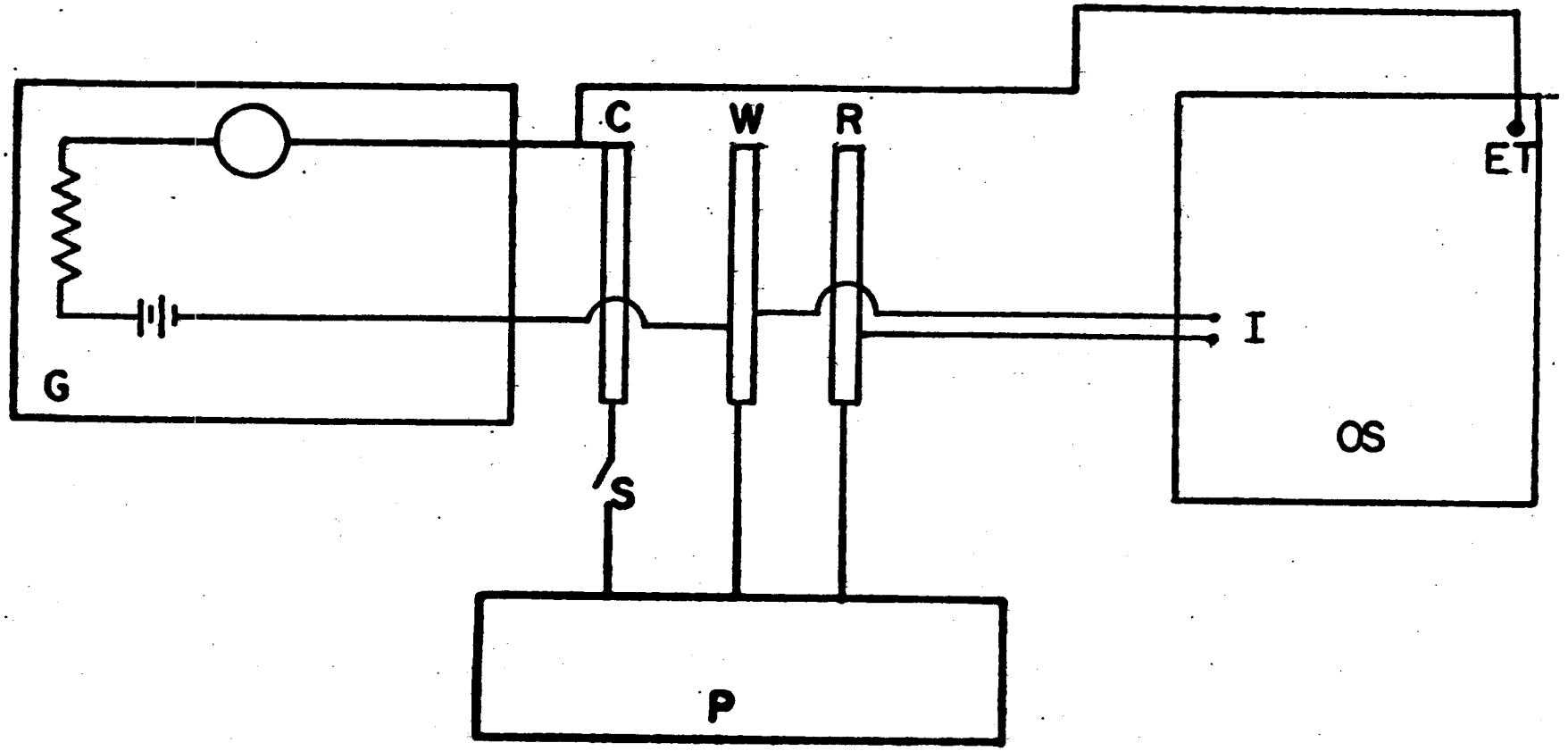

C-Counte Electrode
W-Working Electrode
R- Reference Electrode ($Hg-Hg_2SO_4$)
G-Galvanostat
S-Mercury Switch (normally closed)
P- Potentiostat (Wenking)
OS- Oscilloscope (Tektronix 543)
ET- External Trigger
I- Input

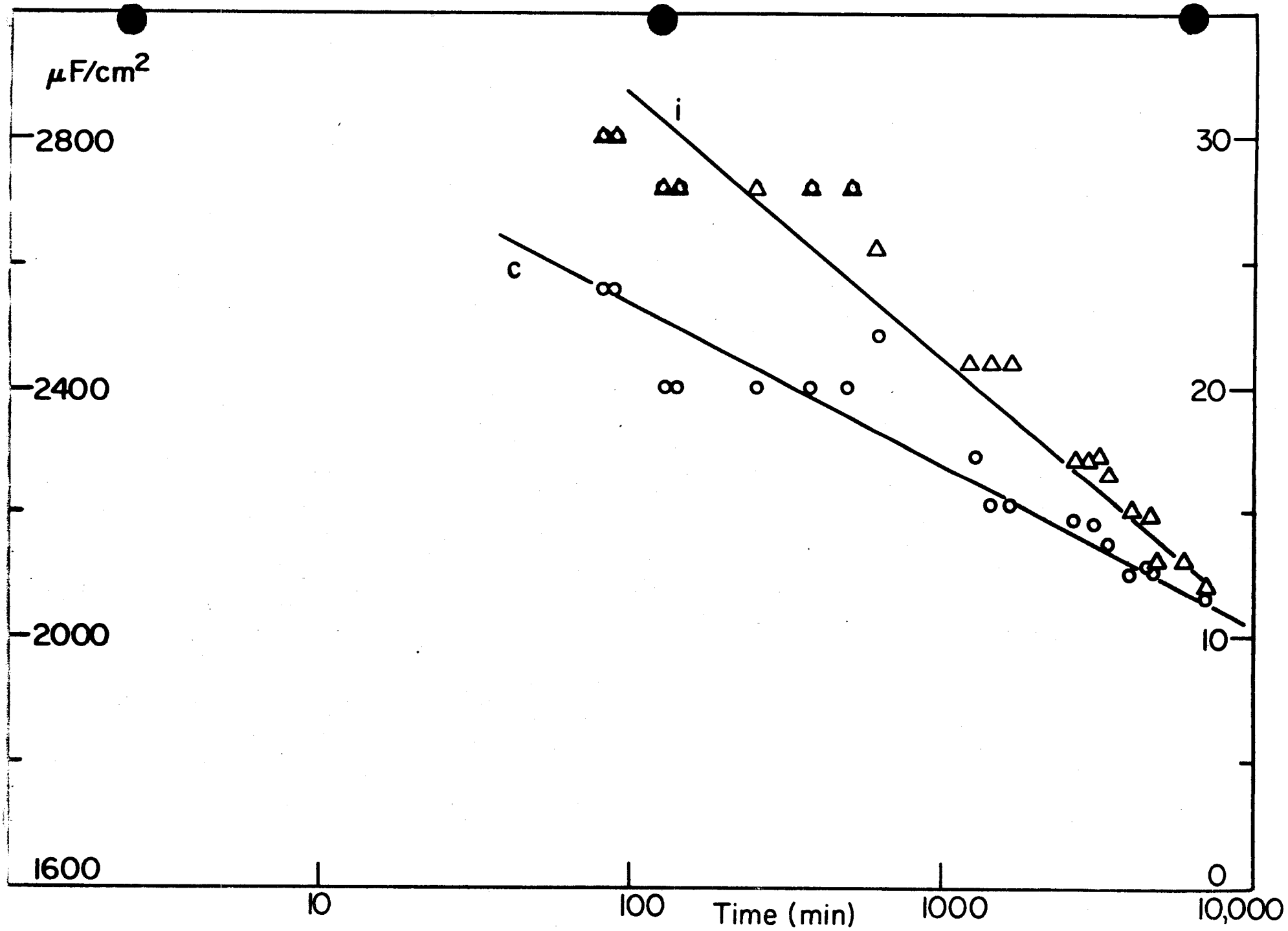

FIG. 5 Variation of current and capacity with time at constant potential

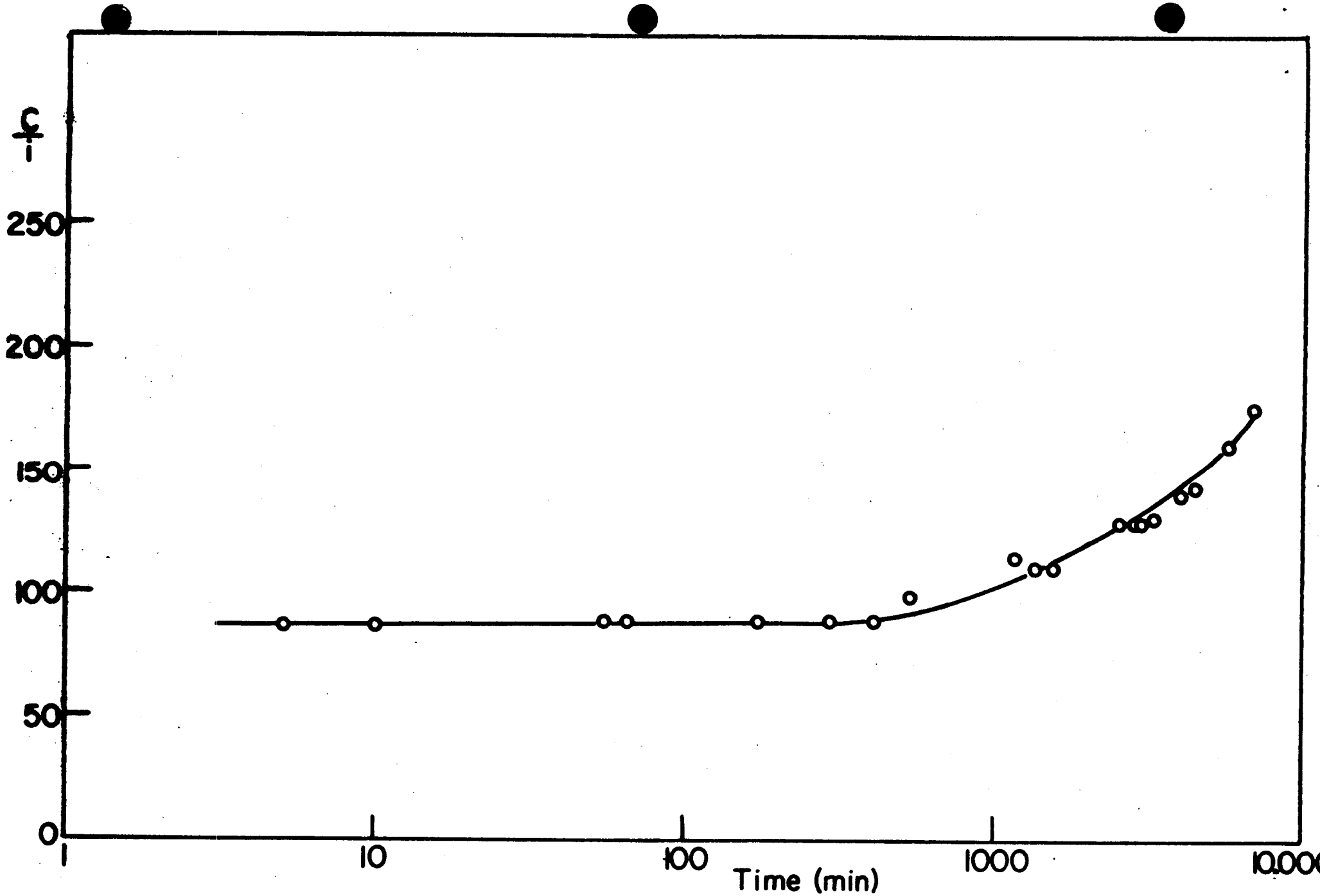

FIG. 6 The ratio C/i as a function of time at constant potential

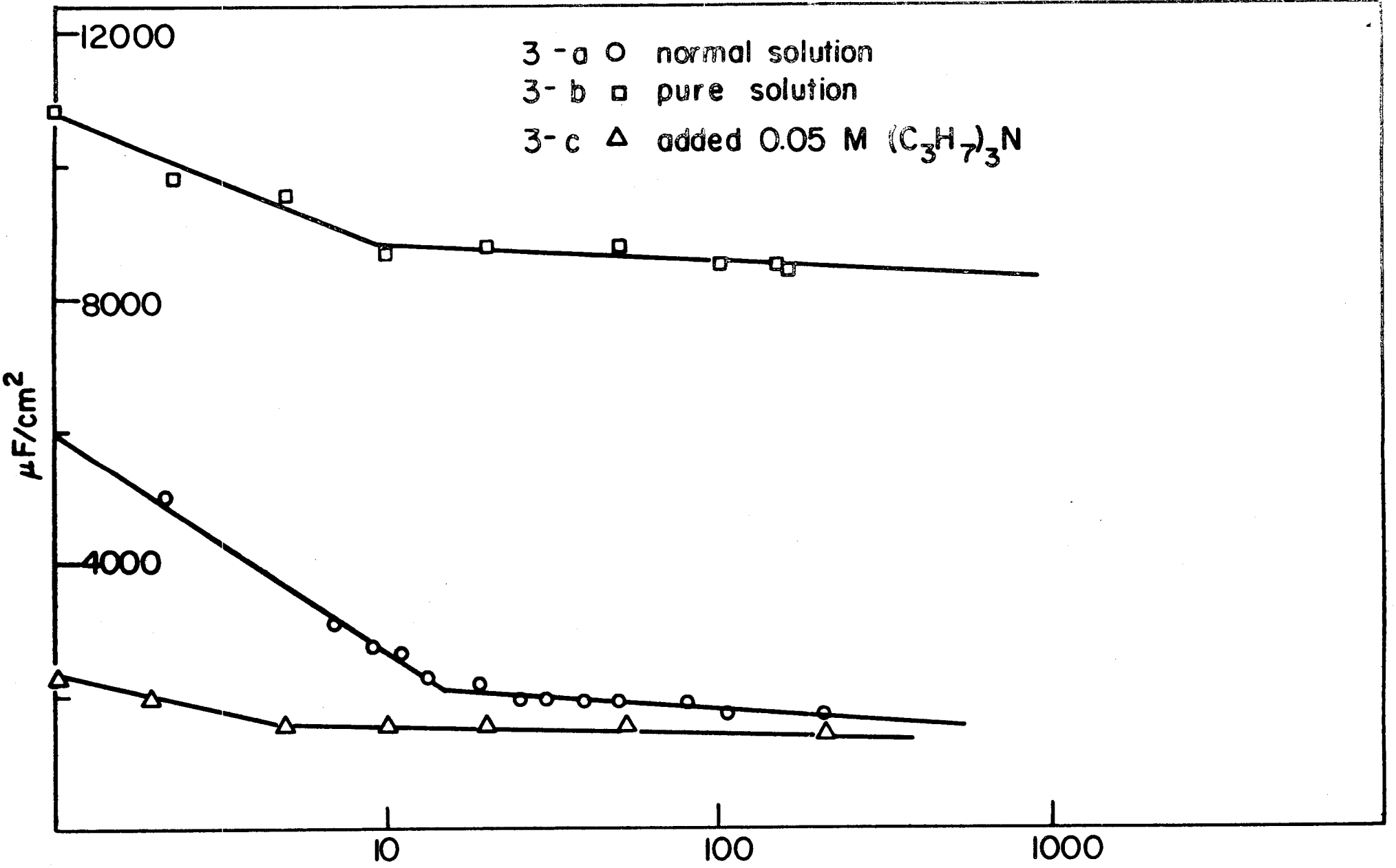

FIG. 7 The effect of impurity on the rate of decrease of capacity with time

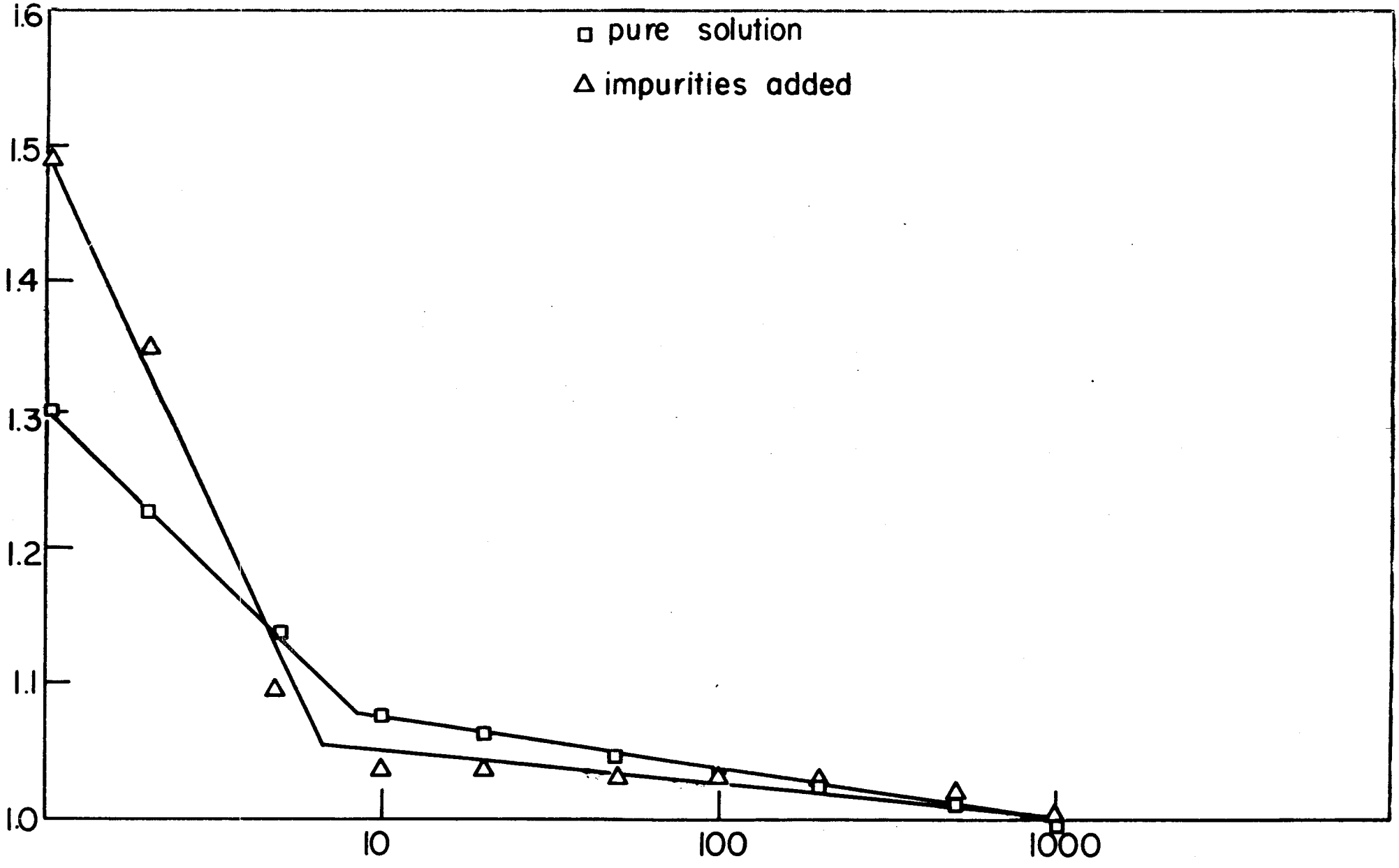

FIG. 8 Normalised plots of C -logt — effect of impurity

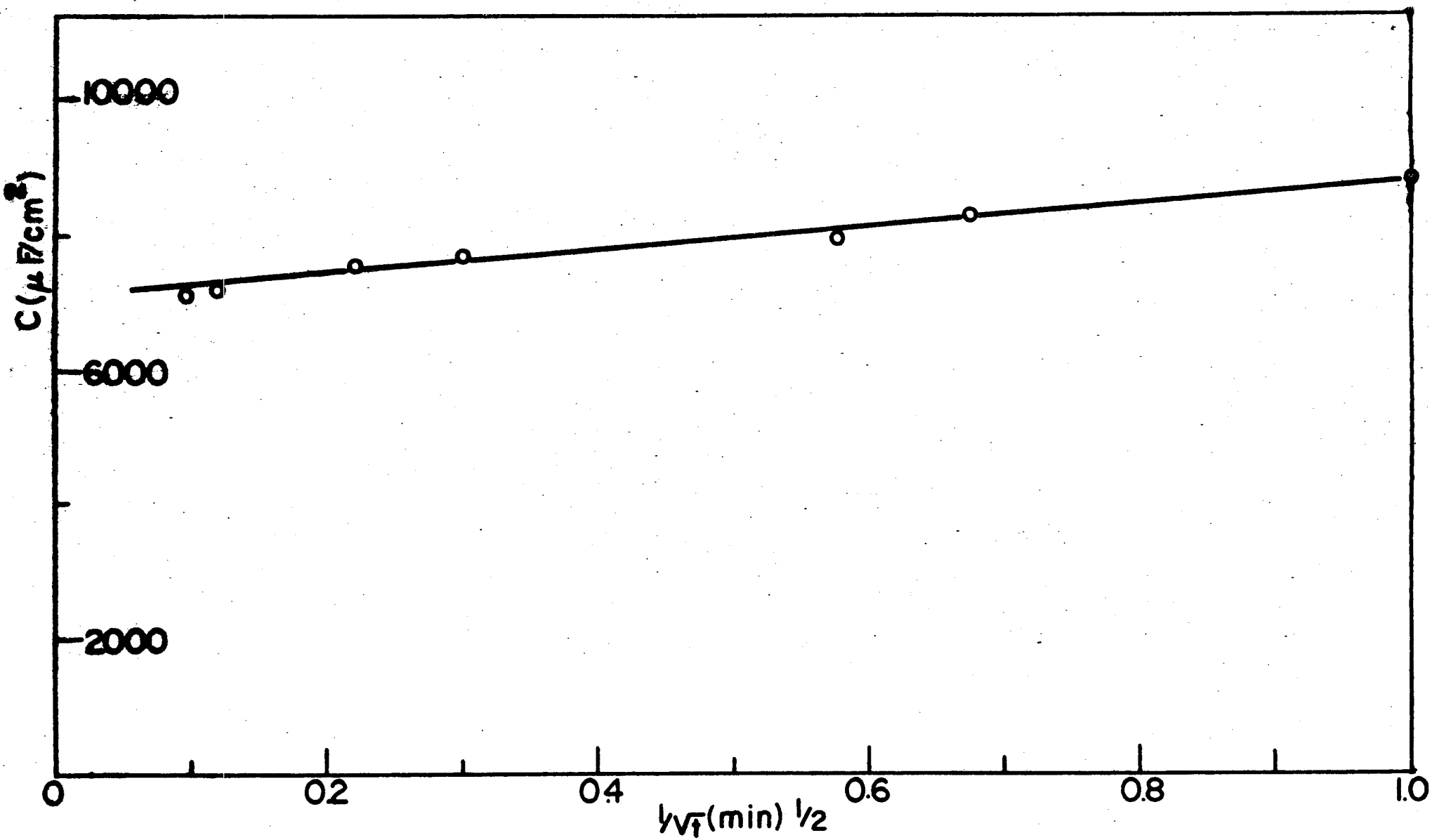

FIG 9a Capacity plotted against $t^{-1/2}$ normal solution

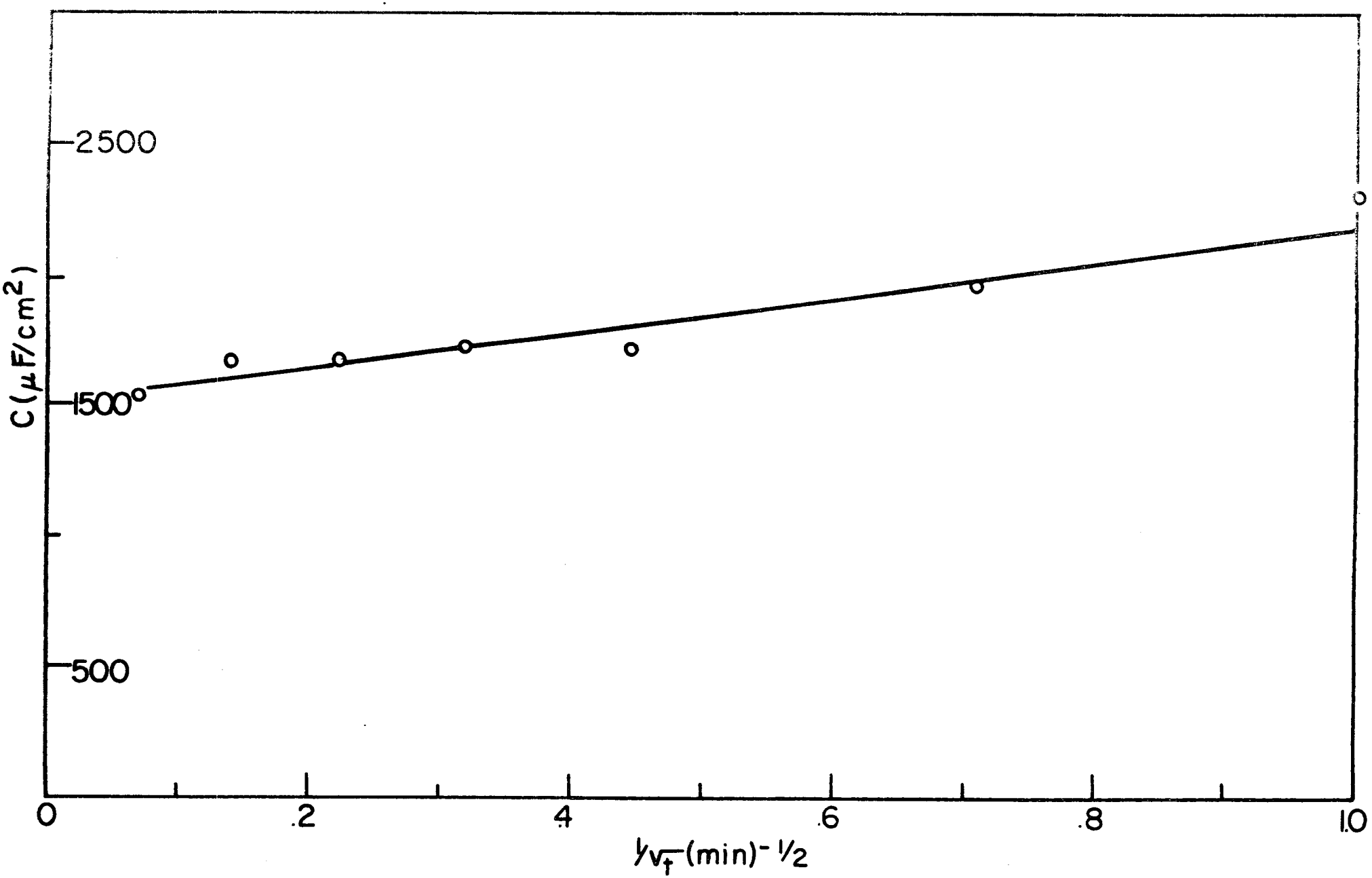

FIG. 9b Capacity plotted against $t^{-1/2}$ (impurities added)

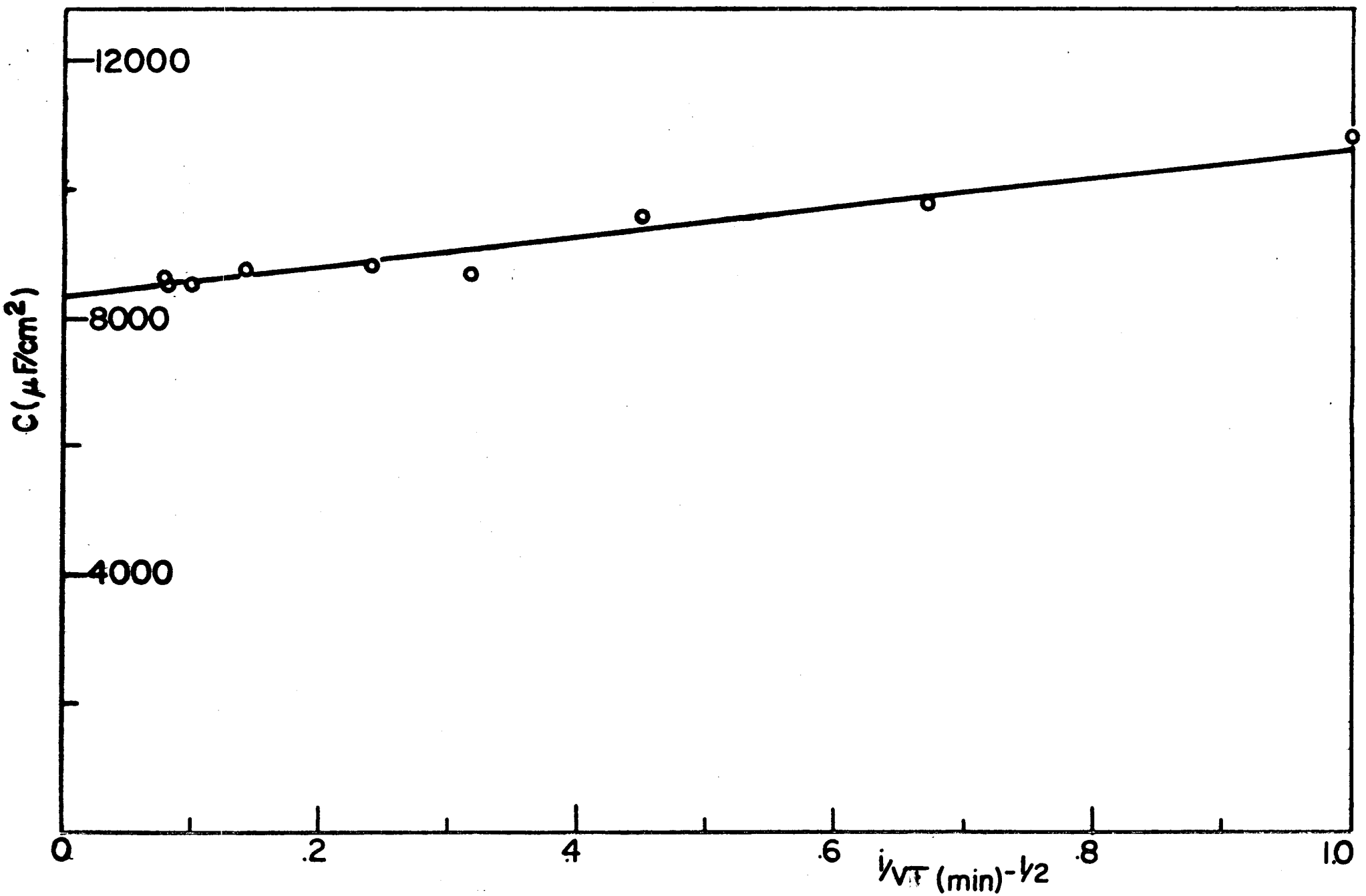

FIG. 9c Capacity plotted against $t^{-1/2}$ (high purity)

V. MODEL POROUS ELECTRODE

A. Transient Behavior

1. The Slit System

The particular geometry chosen for the 'slit' electrode cell was selected so as to give a set of boundary conditions which would be reasonably close to a 'real' porous electrode yet would be mathematically tractable. Because of symmetry, the cell is a two-dimensional system, reducible to one-dimension in most cases, with a plane of symmetry. When operated with a small slit spacing (i.e. $<\sim 0.2$ mm) and the slit completely filled with electrolyte, these conditions should apply.

The cell was arranged with the following conditions: Slit length: 21 mm, slit width, .15 mm, and meniscus length: - 50 mm. The slit was filled with H_2 saturated 1 N H_2SO_4 to the top. The electrode was held potentiostatically at 0 V with respect to H_2 (i.e.$\sim$50 mv with respect to the α-Pd-H electrode used as a reference) until current dropped to zero. (A small random noise current of about 10μA P-P still remains due to imperfect compensation by the potentiostat.) At this point the solution in the slit should be saturated with H_2 and the electrode should be covered with adsorbed H at the proper θ, corresponding to E = 0. At a time, t = 0, a potential step function is applied to the slit electrode with a potentiostat and the current recorded as a function of time on a storage oscilloscope. The potential is then switched off again, the electrode allowed to come to equilibrium and the procedure repeated at a slower sweep speed and increased current sensitivity. Multiple traces

are stored on the oscilloscope, and i-t values are read from photographs of the traces such as are shown in Fig. 1. (Note: 30 sec to 120 Sec must elapse between measurements for equilibrium to be approached sufficiently closely that the values obtained on two successive runs superimpose within $\pm$ 2%, the accuracy of the scope). In this fashion, measurements can be made from $\sim$0.05 msec (the approximate response time of the potentiostat-cell combination) to 10 sec., at which time steady-state operation is approached. (Note the almost flat portion at long times of the trace taken at the slowest sweep speed).

2. Transient Behavior Hypotheses:

It has been fairly well established that the mechanism for the anodic dissolution of H_2 on Pt follows the following reaction path.

(1) $H_2(\text{soln}) \xrightarrow{\text{diffusion}} H_2$ (at surface of electrode)

(2) $H_2(\text{surface}) \longrightarrow 2H_{ads}$

(3) $H_{ads} + H_2O \rightleftharpoons H_3O^+ + e$

where the dissociation reaction (2) is the rate-determining step at steady state. On "activated" Pt surfaces, the i_o for reaction (2) is about 10^{-3} A/cm^2. Parsons (1) has estimated the i_o for step (3) to be about 10^{-1} A/cm^2. At steady state reaction (3) can thus be considered to be in pseudo-equilibrium, but during a transient this is not necessarily true. Consider an electrode initially at $\eta = 0$ which is covered with H_{ads}. When an anodic pulse is applied, current will flow as the H_{ads}

is consumed. If the rate of consumption is greater than the rate at which it will be produced by reaction (2), the coverage, θ, will decrease and the potential will increase to new values where the rates are once again equal. As long as molecular H_2 is supplied to the electrode at a sufficient rate, a new equilibrium value is reached. If the supply of H_2 is limited, as by diffusion, when a thickness equal to the diffusion layer "δ" has been exhausted of molecular H_2, the current will again drop and/or the potential will rise to a diffusion limited value, and (1) becomes the R.D.S.

In the region between 0 V and 0.4 volts, where θ is a function of voltage, varying between $\theta \sim 1$ at 0.0 volts and $\theta \sim 0$ at 0.4 volts, the electrical analogue of the electrode double layer can be considered to be as shown in Fig. 2.

C_{DL} is the usual double layer capacitance of about $20 \mu F/cm^2$, and represents the movement of excess ions into and out of the double layer, and/or the change in distance of the Helmholtz plane to the electrode surface under the influence of an applied field. R_2 is the reaction resistance, $d\eta/di$, of reaction (2), and is highly voltage sensitive. C_{ps} is a pseudo-capacitance, representing the change in voltage produced by a change in θ, which in turn is caused by the current passing through the reaction (3) represented by the reaction resistance R_3 (which is also voltage sensitive).

In many papers, the impedance due to the diffusion resistance of step (1) is pictured as a 'black box' (-W-) called the "Warburg impedance." For AC bridge measurements, at a given frequency, -W- can be represented as where R and C are chosen to

have equal impedances at the given frequency and thus give the correct 45° phase shift. This simple circuit, besides being highly artificial, and having no real physical significance, is of no use in transient work, since a different R and C must be chosen for each instant of time, and the value of C must go to infinity for the steady state. Instead of the Warburg impedance, one can consider the diffusion impedance to be due to an RC transmission line, such as is shown in Fig. 3. This configuration, which is by definition a distributed constant representation and cannot be represented exactly by any finite combination of real R's and C's, can be constructed as a lumped constant approximation to within any desired degree of accuracy, and has a real physical analogue in the diffusion layer. The produce RC of R, the 'resistance' per unit length, and C, the 'capacitance' per unit length, is the analogue of the diffusion coefficient D (where 'R' is the resistance to mass transport under a conc. gradient, and 'C' is the storage capability of the system due to its local concentration. The voltage on the 'common' connection represents the concentration in the bulk of solution. When a pulse is applied (meaning an abrupt change in concentration at the electrode), the concentration at the electrode changes first, and the depletion propagates back to the 'termination' R_T which represents the steady state supply of material at the boundary layer of the convection region, or other source of material.

The total slit electrode is then made up of a series of transmission lines for each incremental area connected as another transmission line extending down the length of the slit where the R is the electrical resistance, and the Z's are circuits as in Fig. 3.

Any number of simplifying assumptions can be made to reduce the system to one which is more easily treatable mathematically, depending on the conditions of measurement.

3. Possible Models and Boundary Conditions

a. Wide slit, high electrical conductance

This system should behave as an ideal flat electrode, and at short times should be equivalent to a simple RC discharge of the double layer and adsorbed H atoms. With an applied potential step, the current should decay as $i = \frac{E}{R} e^{-t/RC}$.

b. Narrow slit, relatively high series resistance of electrolyte

This is represented by a simple transmission line as shown by De Levie[2]. The current decay should fall as $1/t^{1/2}$.

c. Wide slit, high resistance, diffusion control

This is also represented by a similar transmission line with different constants and should decay as $1/t^{1/2}$.

d. Others

Many other configurations are possible but have not yet been analyzed.

4. Experimental Results

The current decay with potentiostatic step functions on a wide ($\sim$ 5 mm) slit are shown in Fig. 4. Four traces are shown corresponding to polarization at 200, 400, 600 and 800 mv. In the lowest two traces, (namely, 200 and 400 mv) the curves are smooth monotonically decreasing functions. The upper two curves (at 600 and 800 mv) start out similarly but have a definite inflection point. Integration under the curves show that the area up to the inflection corresponds ($\pm$ 20%) to the charge that would be obtained from a pseudo-capacitance due to $\theta = 1$ on the surface.

Discharge curves with a narrow slit ($\sim$0.15 mm) such as shown in Fig. 1 show no such inflection. Results of four such transients are plotted in Fig. 5.

Data is plotted as I_{total} vs. log t. Each of the curves consists of 3 - 4 segments. All of them consist of two linear portions of different slopes, followed by an assymptotic tail corresponding to steady state diffusion, and are preceded by a deviation at very short times (i.e. $< 10^{-3}$ to 10^{-4} sec) due to instrumental inaccuracies. (See discussion of error analysis NASA report Oct. 63 to Mar. 64 p. 23-24). The middle two segments show remarkable linearity, especially when it is considered that each curve is a result of the superposition of 5 separate sequential sweeps. The initial maximum current is directly proportional to the applied voltage step, and is probably attributable to some equivalent series solution resistance, and is about 13Ω in the experiments here. (The sheet resistance of the slot electrolyte is about 150Ω/sq. indicating that the reaction at short times takes place over a very small

region at the mouth of the slit.) In Table I are listed the slopes of the various curve segments.

It is interesting to note that both the upper and lower segments of the 400, 600 and 800 mv curves extrapolate to two common points 'A' and 'B'. The curve for 200 mv does not extrapolate to these points.

TABLE I

Step Voltage	Slope 1	Slope 2
200	- 3 ma/decade	- 2.1
400	- 7	- 5.1
600	-14	- 8.25
800	-20.5	-11.8

But, it is probably significant that at 400 mv and above, H_{ads} is completely consumed from the electrode surface, while at 200 mv $\theta \sim 1/2$.

5. Discussion of Results

None of the simple proposed models which on the surface appear to be a reasonable explanation will explain an i vs. $\log t$ behavior, and these experiments yield two such regions. Obviously, then, some hitherto unexpected mechanism is operating in the slit electrode system, which will require more thorough investigation and/or mathematics to uncover.

B. Meniscus Heating Effect

Experimental work has continued on the meniscus heating effect. Motion pictures of the meniscus have been taken on 8 mm film through a Bausch and Lomb stereo microscope, using a Konica movie camera with a microscope attachment. Exposures were determined with a Reichert "Remiphot" microscope exposure meter with an index setting of "-1" and an ocular setting of "4". Pictures were taken at normal speed, and with "stop-motion" photography at about 2 frames per second, giving a "speed up" factor of 5 - 8 times. Several types of meniscus films have been observed and photographed.

1. Uniform Activated Meniscus

When the electrode is immersed in electrolyte and given alternate anodic and cathodic pulses, the electrode becomes more active for a short while (1 - 5 hours), probably because of destruction of adsorbed organics, and removal of oxide films. When the electrolyte is lowered, forming a meniscus, this region is active and gives a uniform droplet region .002 to .005 inches high.

2. Regionally Active Meniscus

After extended operation the electrode surface slowly loses activity, and the active region of the meniscus breaks up and becomes localized.

3. Local Highly Active Regions

As the sputtered film degenerates, small flakes of Pt sometimes dislodge and float in the meniscus region in contact with the primary electrode. This results in a small (.001 - .01 in) hyperactive region around which the droplet activity is especially obvious.

Several hundred feet of film have been taken of these various regions at normal and 'fast' time scales, and are at present being evaluated and edited. A complete quantitative evaluation will probably be impossible, but work is underway for a thorough qualitative explanation and evaluation of the results. It is certainly obvious however that the equation $\nabla^2 T = 0$ must be considered along with $\nabla^2 C = 0$ and $\nabla^2 V = 0$ in the treatment of diffusion in a porous electrode.

REFERENCES

1. Parsons, R., Trans. Faraday Soc., 56, 1340 (1960).

2. De Levie, R., Electrochimica Acta, 8, 751 (1963).

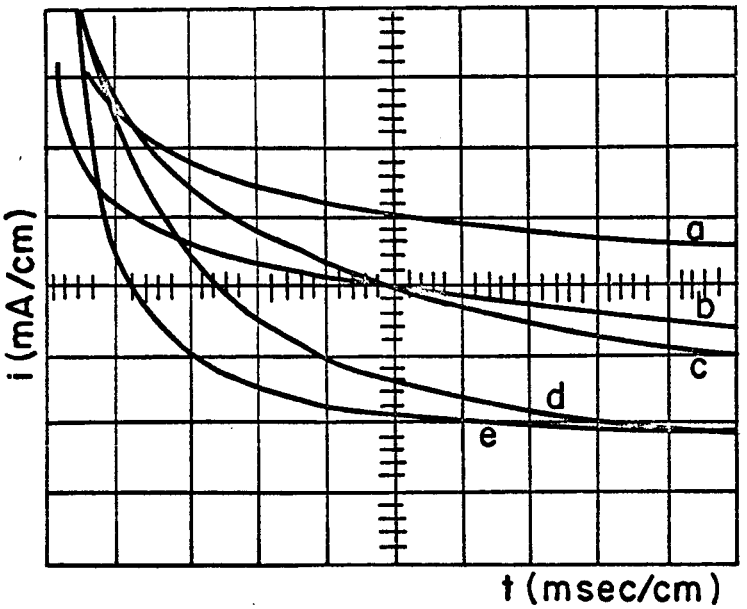

FIG. 1

Typical oscilloscope traces of current transients in 0.15mm slit

a-2 mA/cm	2 msec/cm
b-2 mA/cm	1 msec/cm
c-1 mA/cm	10msec/cm
d-.5 mA/cm	.1sec/cm
e-.2 mA/cm	1sec/cm

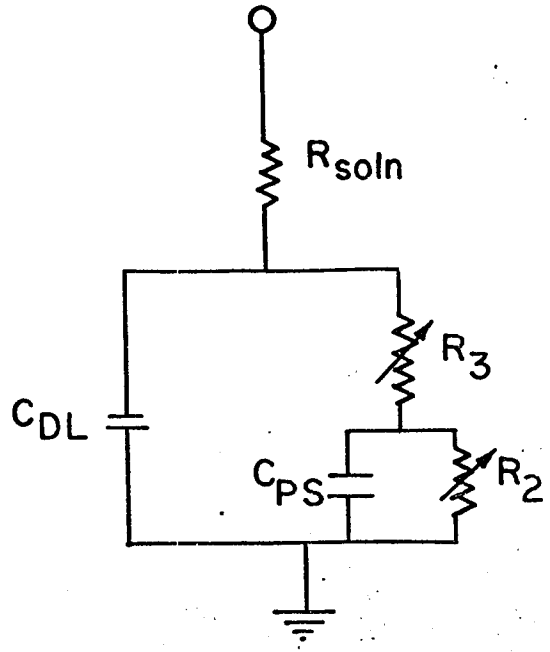

FIG.2
Equivalent circuit for hydrogen dissolution

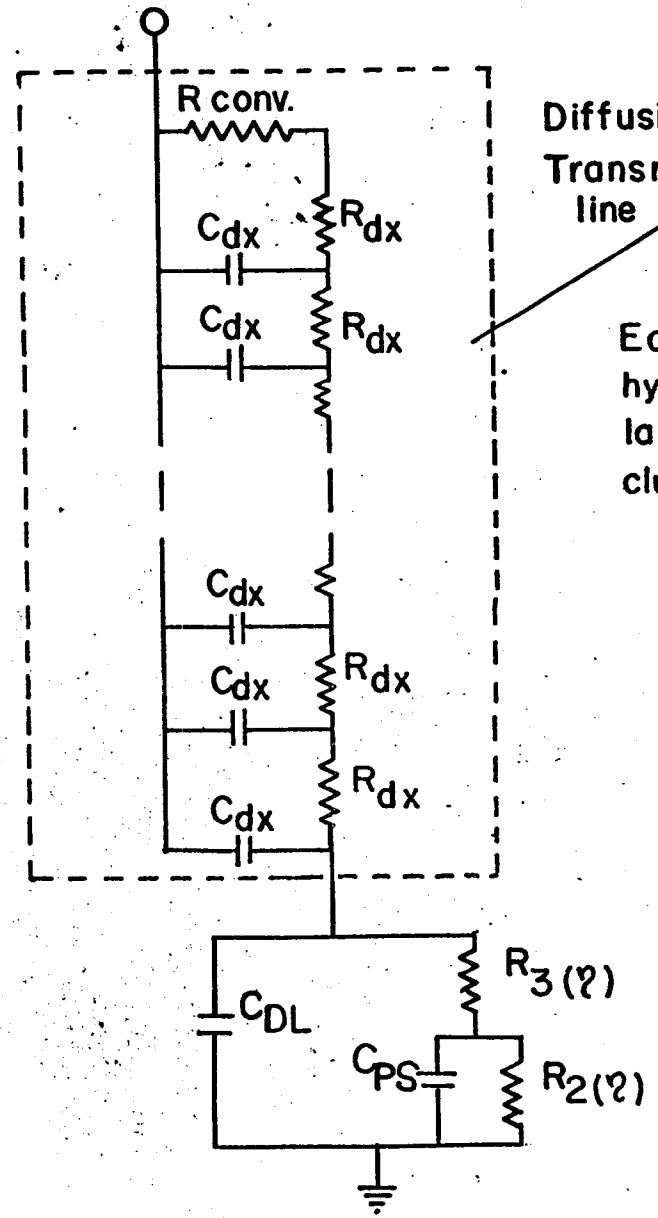

FIG.3
Equivalent circuit for hydrogen dissolution for large voltage steps including diffusion

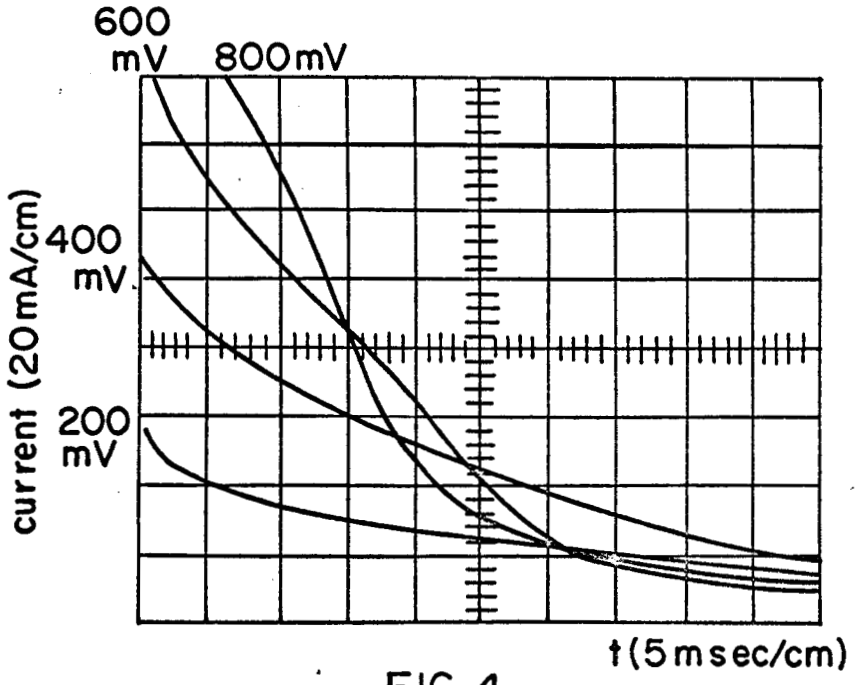

FIG. 4

Oscilloscope traces of current transients in 5mm slit with several potential steps

FIG. 5

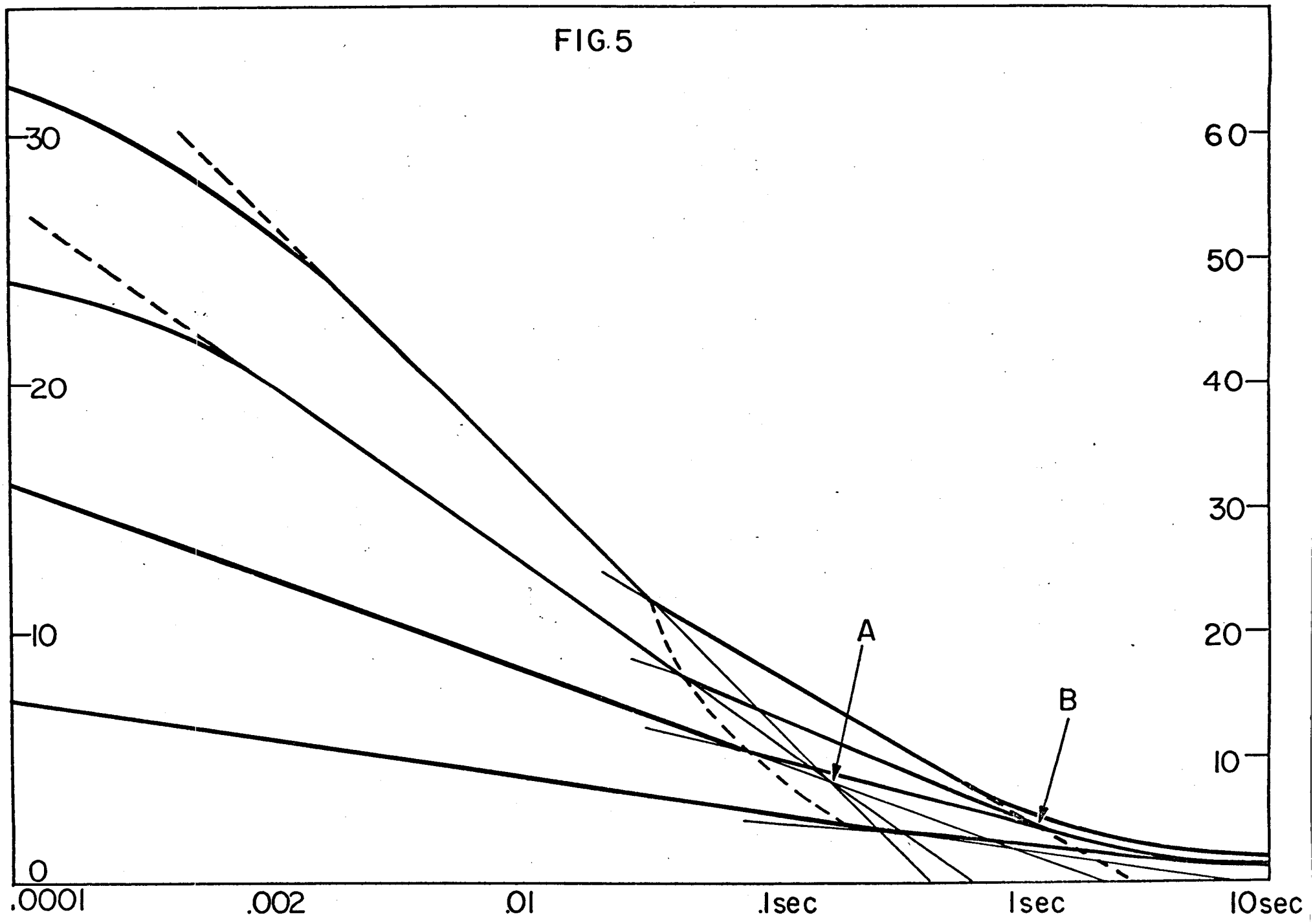

VI. NATURE OF THE CATALYST SURFACE

Ellipsometric Study of Oxide Formation on a Platinum Catalyst Surface

Apart from a study of the influence of the metallurgical characteristics of the catalyst surface on the kinetics of electrode reactions, there is also a vital need to know under what conditions the catalyst can be covered by a surface oxide.

Towards this end, an ellipsometric study of a bright platinum anode immersed in 1 N H_2SO_4, was carried out. At each potential (maintained potentiostatically) the reflected polarized light was studied. From the parameters of the reflected polarized light; the thickness of the oxide film, if any, was determined.

The study has been completed and a report of the work has been submitted for publication (see Appendix 1). Two important conclusions may be mentioned here:

(1) The adsorbed oxygen which has been demonstrated to exist on a platinum anode is transformed into an "oxide" above about 0.975 V (vs. NHE)

(2) Thereafter, the "oxide" grows linearly with potential; the ellipsometric thickness-potential curve agreeing with that determined coulometrically.

APPENDIX I

Journal of Electroanalytical Chemistry

Short Communication

ELLIPSOMETRIC STUDY OF OXYGEN-CONTAINING FILMS ON PLATINUM ELECTRODES

This brief communication describes the main results which have emerged from an ellipsometric study of the oxygen-containing films on bright platinum sheet-anodes in acid solutions (1 N H_2SO_4). Ellipsometry is a direct and in situ optical method of examining films on reflecting surfaces. It is based on a study of the changes which surface films produce on the polarization state of a light beam reflected from a metallic mirror.

The particular ellipsometric method used[1] is that of a quantitative study of films held in a steady-state condition by means of a potentiostat (Fig. I). The parameters of the reflected elliptically polarized light were determined while maintaining the potential of a reflected platinum sheet-anode at various values. From these parameters, the thickness of the film was calculated using standard ellipsometric procedures.[2]

The dependence of average film thickness on potential is shown in Fig. 2. The thickness-potential plot shows that: (i) at potentials less positive than about 0.98 V (vs. N.H.E.), there is no ellipsometric evidence of a film although the sensitivity of the technique is about 0.1 Å; (ii) a film (of average thickness $\sim$ 0.2 Å) "comes on" suddenly at about +0.980 $\pm$ 0.010 V; (iii) and thereafter the film thickness increases linearly with potential (a result which is in striking agreement with those of coulometry[3-6]).

Computer analysis of the ellipsometric data shows that the refractive index (n_F^*) of the film is a complex quantity, i.e., $n_F^* = n_F + ik$. The real part (n_F) of the complex refractive index is 3.3. The imaginary part is the absorption coefficient (k) which is a measure of the conductivity of the film at optical frequencies. The results indicate that this conductivity at optical frequencies (in this case of the film on platinum) is of the same order as that of a metal, judging from the order of magnitude of the same optical-frequency quantity for semi-conductors and metals.[7,8]

The ellipsometric detection of a surface film depends on the optical constants (n_F^*) of the film being sufficiently different from those of the surrounding medium. It is suggested, therefore, that the difference between chemisorbed oxygen and water is too small to make a chemisorbed oxygen film register in the ellipsometer. When, however, platinum joins with oxygen to form a new phase, the optical constants between this "oxide" and the surrounding water are adequate to produce an ellipsometric effect. The average thickness of 0.2 Å of this platinum "oxide" film is interpreted in terms of a "partial" coverage of a mono-layer of oxide.

Acknowledgements

The authors thank Miss W. Visscher and Dr. M. A. V. Devanathan for help and discussion in the preliminary experiments and the University Computer Center for their assistance. The financial support of the Aeronautical Systems Command and the National Aeronautics and Space Administration, Contract No. NsG-325 and U.S. Army Electronics Laboratories,

Fort Monmouth, New Jersey, Contract No. DA 36-039 SC-89921 is gratefully acknowledged.

One of us (A.K.N.R.) thanks the Council of Scientific and Industrial Research, India, for the grant of a Leave of Absence.

Electrochemistry Laboratory,
University of Pennsylvania,
Philadelphia 4, Pa., (U.S.A.)

A. K. N. Reddy
M. Genshaw
J. O'M. Bockris

1. A. K. N. Reddy and J. O'M. Bockris, Proceedings of the Symposium on the Ellipsometer and its Use in the Measurement of Surface Films, National Bureau of Standards, Publication No. 256, Washington, D.C., September, 1964.

2. A. B. Winterbottom, Det. Kgl. Norski Vidensk. Selsk. Skr. nv 1 (1955).

3. F. G. Will and C. A. Knorr, Z. Elektrochem., 64 (1960) 258.

4. H. A. Laitinen and C. G. Enke, J. Electrochem. Soc., 107 (1960) 773.

5. M. W. Breiter, Electrochim. Acta., 7 (1962) 601.

6. W. Visscher and M. A. V. Devanathan, J. Electroanal. Chem., 8 (1964) 127.

7. M. Born and E. Wolf, Principles of Optics, Pergamon Press 1959, Chap. XIII.

8. R. J. Archer, J. Electrochem. Soc., 104 (1957) 619.

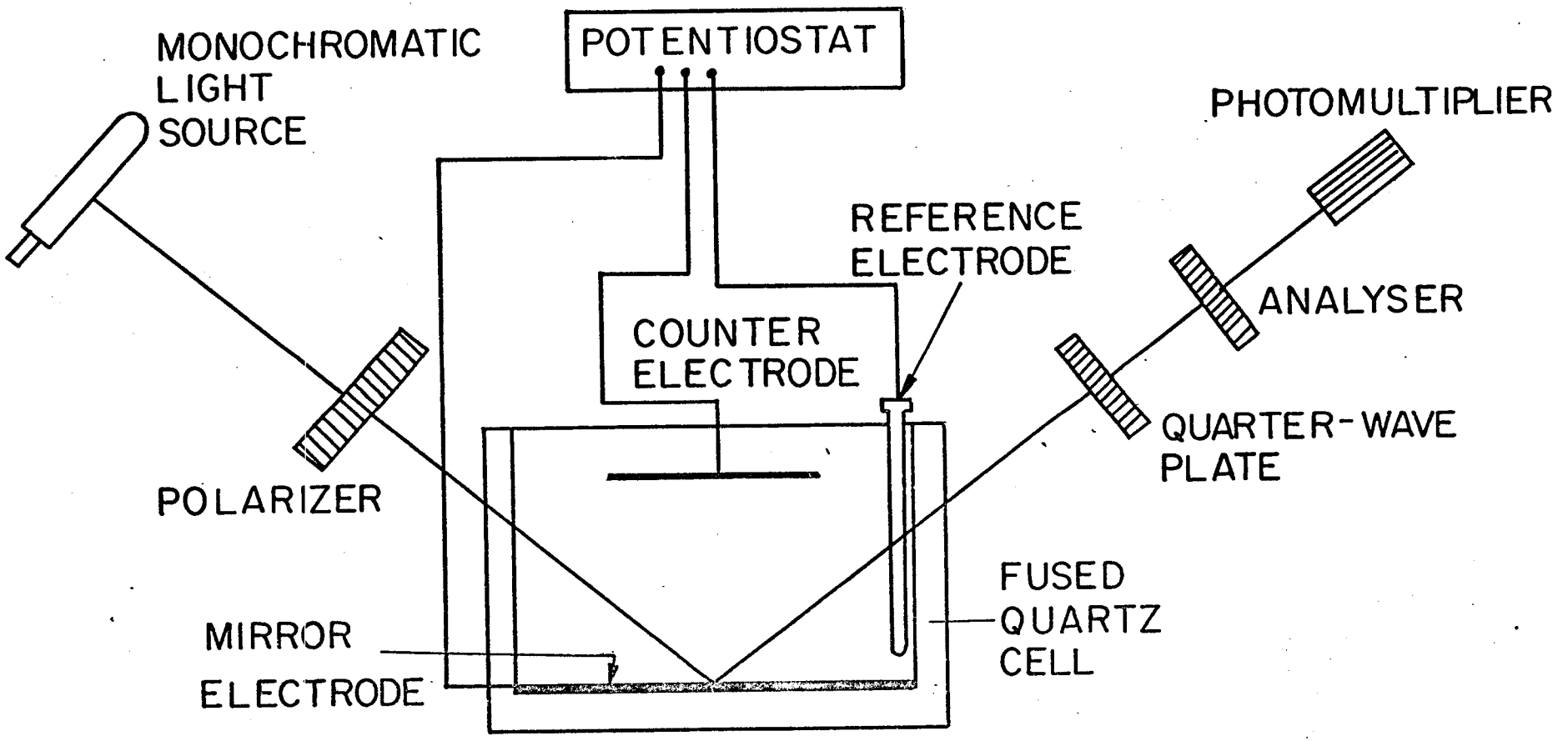

FIG.1

Experimental Arrangement

FIG.2

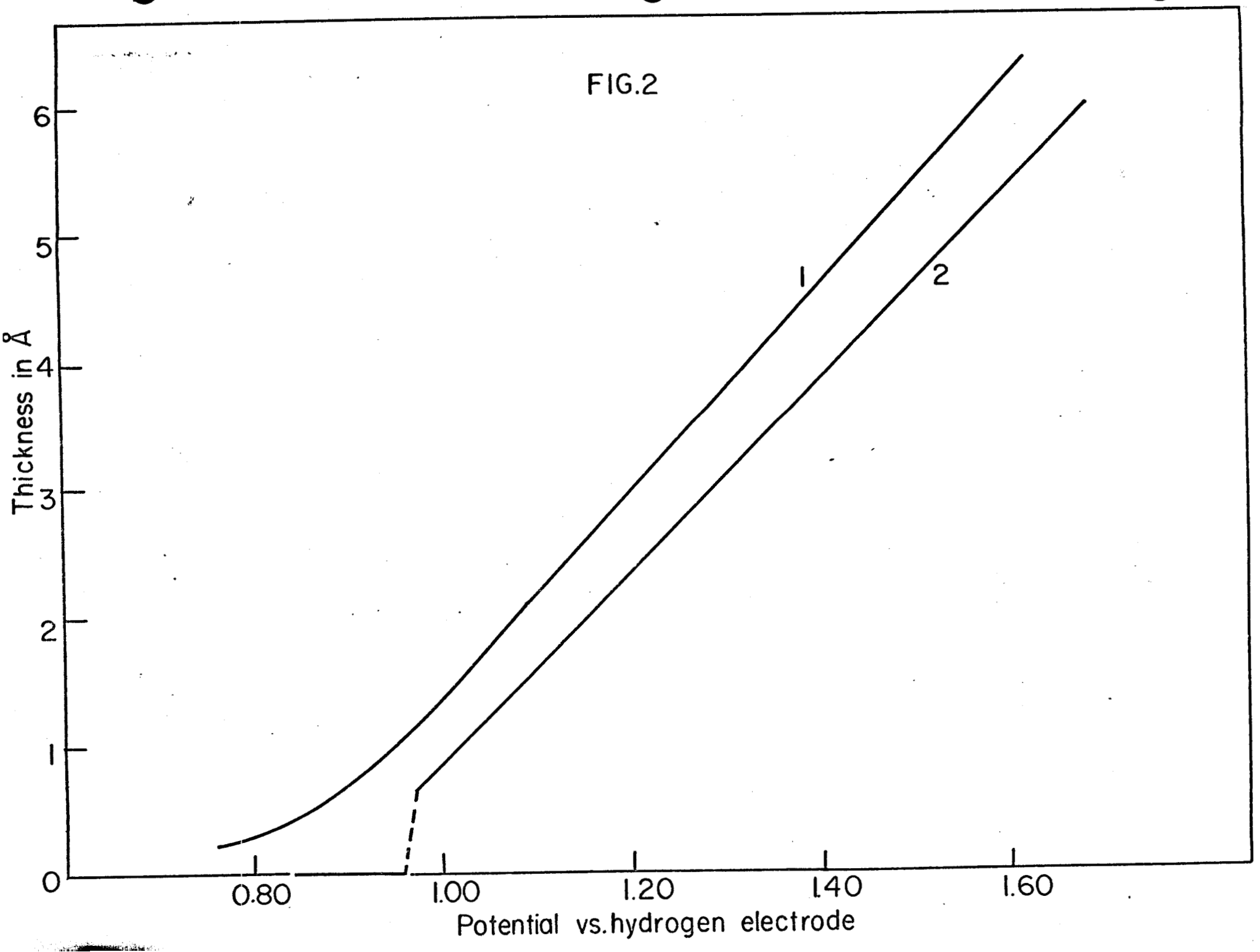
Thickness in Å
0
1
2
3
4
5
6
0.80
1.00
1.20
1.40
1.60
Potential vs. hydrogen electrode
1
2